11-4-2021

Synthesis, Evaluation, and Characterization of an Ergotamine Imprinted Styrene-Based Polymer for Potential Use as an Ergot Alkaloid Selective Adsorbent

Manoj B. Kudupoje
University of Kentucky, mkudupoje@alltech.com

Eric S. Vanzant
University of Kentucky, evanzant@uky.edu

Kyle R. McLeod
University of Kentucky, kyle.mcleod@uky.edu

Alexandros Yiannikouris
Alltech Inc.

Synthesis, Evaluation, and Characterization of an Ergotamine Imprinted Styrene-Based Polymer for Potential Use as an Ergot Alkaloid Selective Adsorbent

Digital Object Identifier (DOI)
https://doi.org/10.1021/acsomega.1c02158

Notes/Citation Information
Published in *ACS Omega*, v. 6, issue 45.

ACS OMEGA

http://pubs.acs.org/journal/acsodf

Article

Synthesis, Evaluation, and Characterization of an Ergotamine Imprinted Styrene-Based Polymer for Potential Use as an Ergot Alkaloid Selective Adsorbent

Manoj B. Kudupoje,* Eric S. Vanzant, Kyle R. McLeod, and Alexandros Yiannikouris

Cite This: *ACS Omega* 2021, 6, 30260−30280

Read Online

ACCESS | Metrics & More | Article Recommendations

ABSTRACT: Alkaloid toxicities negatively impact livestock health and production. To assess alkaloid occurrences, adsorbent technologies may offer effective means to their extraction and isolation from a complex feed matrix. In this study, molecularly imprinted polymers (MIPs) were synthesized and evaluated for their specificity of binding to various ergot alkaloids. Co-polymers of styrene and hydroxyethyl methacrylate were synthesized in the absence or presence of an ergotamine (ETA) template, yielding non-imprinted polymer (NIP) and molecularly imprinted polymer (MIP), respectively. The influence of parameters such as pH, temperature, and initial concentration on the adsorption of ergot alkaloids was evaluated along with their application as solid phase extraction materials. Chemical and morphological properties were characterized. Adsorption was generally greater for MIP compared to NIP. Cross-reactivity with related alkaloids existed due to similarities in structure and functional groups and was dependent on the type and concentration of alkaloid and polymer type (alkaloid type × concentration × product; $P < 0.05$). The pH of the medium had no influence on the binding properties of polymers toward ETA within a pH range of 2−10. Binding was independent of temperature between 36 and 42 °C. When kinetics of adsorption were evaluated, the Langmuir isotherm had a better fit ($R^2 > 0.95$) to adsorption equilibrium data than the Freundlich equation. The maximum amounts adsorbed (Q_o) from the Langmuir model were 8.68 and 7.55 μM/g for MIP and NIP, respectively. Fourier transform infrared, scanning and tandem electron microscopy, and Brunauer−Emmett−Teller analysis confirmed a highly porous MIP structure with a greater surface area compared to NIP. Binding characteristics evaluated with computational strategy using molecular docking experiments and *in vitro* in a complex media (rumen fluid) indicated a stronger ETA adsorption by the tested composition selected among other polymeric materials and affinity of MIP compared with NIP. This study suggested the possible utility of MIP as a solid phase extraction sorbent for applications in analytical chemistry or sensing devices tailored to track ergot alkaloid incidence and the fate of those alkaloids in complex ruminal digestive samples.

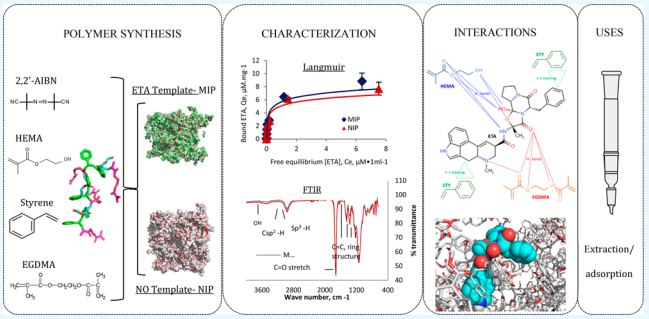

INTRODUCTION

Tall fescue (*Lolium arundinaceum*) is a cool-season perennial grass widely used as forage in the eastern and northwestern United States. In the context of animal production, the popularity of tall fescue is mainly due to its ability to withstand extreme stress conditions. Animal industries in areas dominated by fescue have suffered significant financial losses due to fescue toxicosis that is caused by a family of alkaloids produced in endophyte-infected tall fescue.[1] Ergot alkaloids are secondary metabolites produced by the endophyte *Epichloë coenophiala*, a symbiotic fungus of tall fescue that helps the grass resist abiotic (e.g., extreme weather) and biotic (e.g., nematode) stresses.[2] Ergot toxicities have been reported, including "fescue toxicosis" in animals grazing endophyte-infected tall fescue[3,4] and "rye grass staggers" in sheep consuming *Acremonium lolii* infected ryegrass. Chemically, ergot alkaloids consist of an ergoline ring and its amine derivatives with two or more functional groups.[5] Ergot toxicity arises in animals because of binding of these alkaloids to α-1 and α-2 adrenergic, D_2 dopaminergic, and a family of 5-HT2 serotonergic receptor sites.[6−9] Toxicological effects range from weight loss in mild cases to death in most severe cases depending on the environmental stress factors and level of exposure to alkaloids.[8−10] Toxicity symptoms become more severe when co-occurrence of different alkaloids is encoun-

Received: April 23, 2021
Accepted: October 1, 2021
Published: November 4, 2021

tered. However, in most cases, ergovaline has been reported as the most abundant[11] alkaloid in endophyte-infected tall fescue and is considered the putative cause for most cases of alkaloid toxicity. Due to the extent of financial loss (>$1 billion/year[8]) and the dependence of animal industries on fescue, monitoring and mitigation strategies are required to control animal exposure to such contaminants.

Assessing contamination levels of ergot alkaloids can be achieved through high-performance liquid chromatography−tandem mass spectrometry (LC−MS/MS) with simultaneous quantification of major alkaloids as well as their epimers at low concentrations.[12] High-throughput and sensitive LC−MS/MS methods are based on multiple reaction monitoring by measuring both target analytes and their specific fragments while accounting for signal suppression or enhancement due to the matrix effect by using matrix matched calibration or, when available, stable-isotope internal standard dilutions.[13,14] The accuracy and precision of analysis can be dramatically improved by using purification or dilution strategies to mitigate the impact of the sample matrix. Several sample cleanup techniques have been adopted, including the use of liquid−liquid extraction,[15] immunoaffinity columns,[16] filtration, centrifugation, and solid phase extraction (SPE). Among these techniques, the SPE method is gaining prominence with the advent of new SPE materials called molecularly imprinted polymers (MIPs)[17] due to their selectivity and recovery rate for targeted analytes.

Molecular imprinting is a technique for synthesizing macromolecular polymers (molecularly imprinted polymers; MIPs) with specific binding pockets and multifunctional receptor groups that can form complexes with the targeted molecule(s).[18,19] These template-based cavities will have high binding affinities for that specific template and closely related molecular species.[20] The structural and molecular complementarity between the imprinted polymer and the targeted template molecule governs the specificity of its molecular recognition. This technology has been utilized in the extraction and removal of impurities in water waste management,[21] in drug delivery,[22] and in a range of biotechnological applications.

An imprinted polymer toward lysergic acid diethylamide (LSD) that was synthesized using methacrylic acid (MAA) functional monomers and ergometrine as a template[23] showed 82% extraction recovery of LSD analogs from hair and urine samples. Similarly, an MIP synthesized from an MAA monomer cross-linked with ethylene glycol dimethacrylate (EGDMA) in chloroform further imprinted with metergoline as a template exhibited high selectivity toward the same when compared to non-imprinted polymers (NIPs).[17] However, cross-reactivity with certain polycyclic compounds occurred with both MIP and NIP. Most imprinting studies have used acrylates as the functional monomer, and studies using styrene-based imprinted polymers, especially for ergot alkaloids, are limited.

The goal of the present study was to develop an ergotamine-imprinted styrene-hydroxyethyl methacrylate (HEMA)-based MIP that can interact with different ergot alkaloids possessing common ergoline ring structures. This report details the morphological and physical characteristics and template rebinding of molecularly imprinted co-polymers using commonly used adsorption isotherm models. This work also aimed at identifying the nature of the molecular interactions between the polymer and template to understand the specificity, selectivity, and binding site properties. Such solid phase adsorbing materials may have utility in the extraction and cleanup of complex feed or fluid matrixes.

RESULTS

Molecularly Imprinted Polymer Synthesis. This research focused on evaluating the adsorption properties of MIP along with their physical and morphological characterization. With the formulation used, 35 g of imprinted polymer was synthesized. The washings accounted for a total removal of 96% of the bound ETA from the polymer matrix (1.45 g out of 1.51 g ETA bound to the polymer). The recovery of ETA with the initial acidic methanol washes was low, and the template removal was maximal after several washes with methanol and acetonitrile. Quantitatively, most template removal occurred over the five methanol washes. The remaining template bound in the polymer (4%) suggested the immobilization of ETA in the polymer matrix due to the strong interaction between the template and polymer and/or to the permanent entrapment of ETA in the polymer.

Morphological Characterization of Polymer. *Nitrogen Sorption Porosimetry.* An increase in the volume of N_2 adsorbed with the increase in relative pressure of nitrogen into pores of the polymer was observed (Figure 1). A

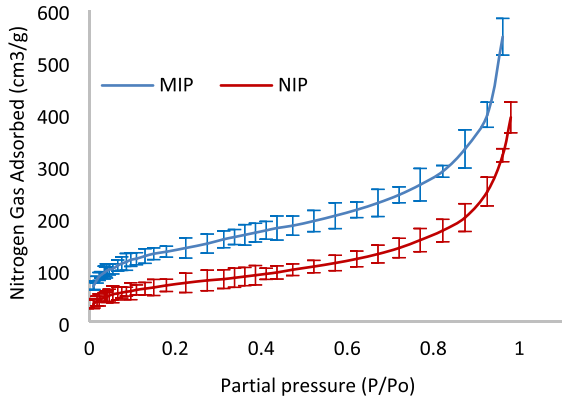

Figure 1. Adsorption isotherms in the mesoporous systems of styrene-based molecularly imprinted (MIP) and non-imprinted (NIP) polymers. Adsorption excess is given in units of cm_3/g adsorbate, plotted against relative pressure.

significant proportion of mesopores (5−8 nm pore size) was evident in both polymers with a cumulative pore volume of 1.1 and 0.613 cm^3/g for MIP and NIP, respectively (Table 1). A comparatively large BET surface area and pore volume of MIP

Table 1. Surface Area, Pore Volume, and Pore Size of Syrene-based Molecularly Imprinted (MIP) and Non-imprinted (NIP) Polymers Using Brunauer−Emmett−Teller (BET) and Barrett−Joyner−Halenda (BJH) Methods

	MIP	NIP
BET surface area (m^2/g)	431.4 ± 11.6	213.1 ± 3.4
BJH cumulative pore volume (cm^3/g)		
0.5 and 300 nm diameter	1.11 ± 0.04	0.61 ± 0.03
1 and 300 nm diameter	0.95 ± 0.03	0.54 ± 0.02
BJH average pore diameter (nm)		
adsorption	5.41 ± 0.06	6.21 ± 0.23
desorption	7.77 ± 0.17	7.57 ± 0.26

https://doi.org/10.1021/acsomega.1c02158
ACS Omega 2021, 6, 30260−30280

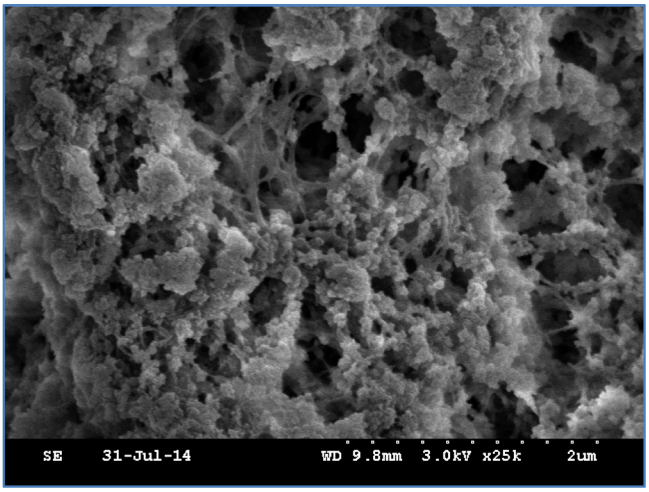

A.SEM _ MIP

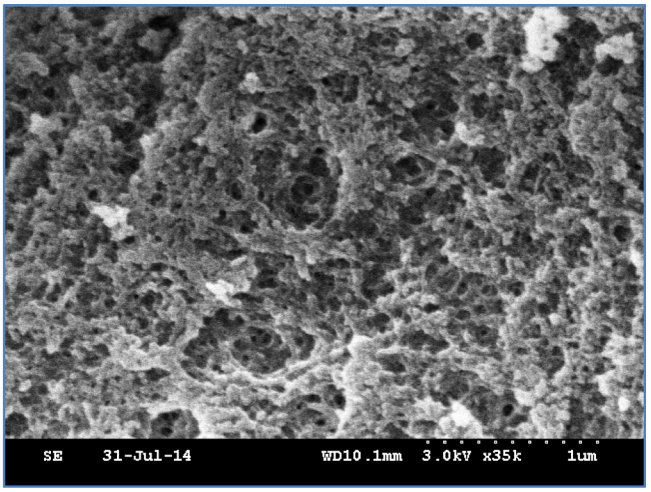

B.SEM_NIP

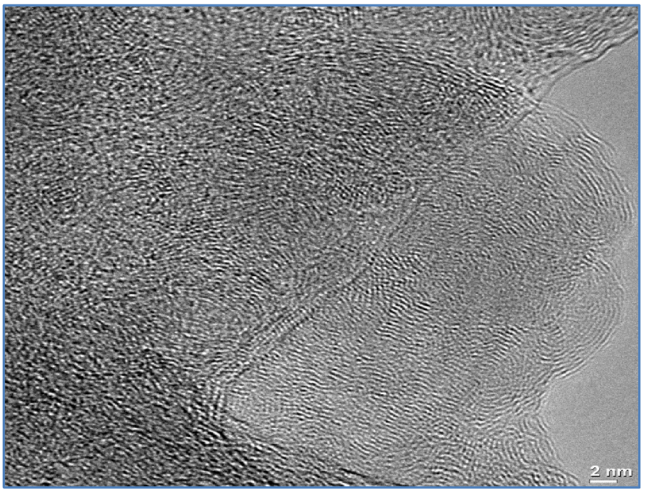

C.TEM_MIP

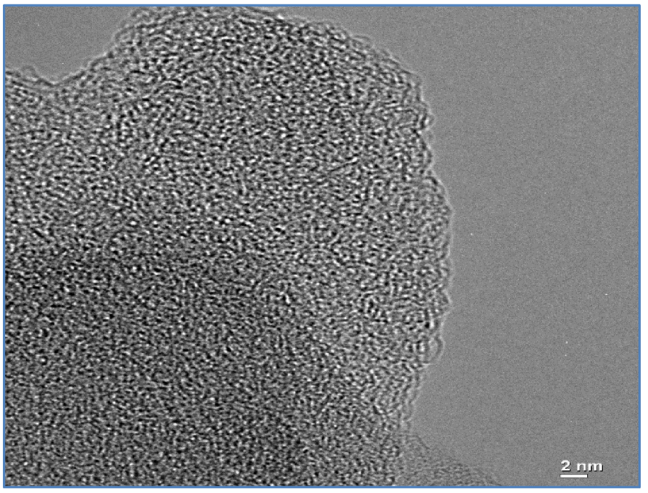

D.TEM_NIP

Figure 2. Scanning electron (SEM) and transmission electron microscopy (TEM) images of styrene-based molecularly imprinted (MIP) and non-imprinted (NIP) polymer. (A, B) SEM of MIP and NIP. (C, D) TEM of MIP and NIP.

(431 m^2/g and 0.9−1.1 cm^3/g, respectively) were noticed compared to NIP (213 m^2/g and 0.54−0.61 cm^3/g, respectively). The specific surface area and pore volume were higher for MIP compared to NIP.

Microscopy. The SEM and TEM micrographs of MIP and NIP in their dry form revealed non-uniform dispersions of particles with irregular morphologies (Figure 2A,B). NIP had a more regular structure than MIP. However, the surface of MIP exhibited more cavities than NIP. The morphology of polymers evaluated by TEM (Figure 2C,D) suggested that both polymer particles were amorphous in nature.

Dynamic Light Scattering. Trimodal distributions of particle size were observed for both polymers in water and in 5% aqueous methanol (Figure 3). Irrespective of the media, most particles were in the range of 5 to 90 μm with a peak in the range of 38−57 μm. In deionized water, a slight aggregation was noticed. This observation indicated that polymer sizes when dispersed in adsorption media were similar between MIP and NIP.

Adsorption Studies. *Isothermal Adsorption Study.* Langmuir and Freundlich constants derived from isothermal adsorption data are presented in Table 2. Figure 4a,b

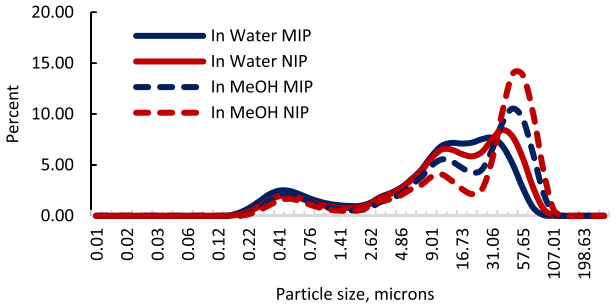

Figure 3. Hydrodynamic particle size distribution (%) molecularly imprinted (MIP, blue) and non-imprinted (red) polymers in water (solid line) and in 5% methanol (dotted line) by dynamic light scattering (DLS) measurements.

represents Langmuir and Freundlich plots, respectively, for the adsorption of ETA to polymers. Statistically, for both models, residuals were randomly scattered around zero, and normal probability plots suggested that the random errors affecting the adsorption process were normally distributed. Even though both models had good fit (R^2 > 0.9), the Langmuir model provided a better fit than the Freundlich

https://doi.org/10.1021/acsomega.1c02158
ACS Omega 2021, 6, 30260−30280

Table 2. Langmuir and Freundlich Isotherm Adsorption Parameters of Ergotamine (ETA) to Styrene-based Molecularly Imprinted (MIP) and Non-imprinted (NIP) Polymer[a]

	Langmuir				Freundlich			
	Q_o (μmol/g)	K_L (L/g)	R_L	R^2	K_f (μmol/g)	$1/n$	n	R^2
MIP	8.68 ± 0.80	0.37 ± 0.14	0.38	0.95	2.48 ± 0.41	0.31 ± 0.04	3.16	0.94
NIP	7.55 ± 0.61	0.43 ± 0.01	0.37	0.96	2.40 ± 0.39	0.29 ± 0.04	3.37	0.92
equation		$q_e = \frac{Q_o K_L C_e}{1 + K_L C_e}$	$R_L = \frac{1}{\frac{1}{1 + K_L C_o}}$		$q_e = K_f C_e^{1/n}$			

[a] q_e: amount adsorbed, μmol/g; K_L: Langmuir adsorption constant; Q_o: maximum amount adsorbed (μmol/g); C_o: initial concentration of adsorbate (μmol/L); C_e: equilibrium concentration of adsorbate (μmol/L); K_f: adsorption capacity factor; and $1/n$: adsorption intensity or surface heterogeneity index. Data represent mean ± standard error of the mean (n = 3).

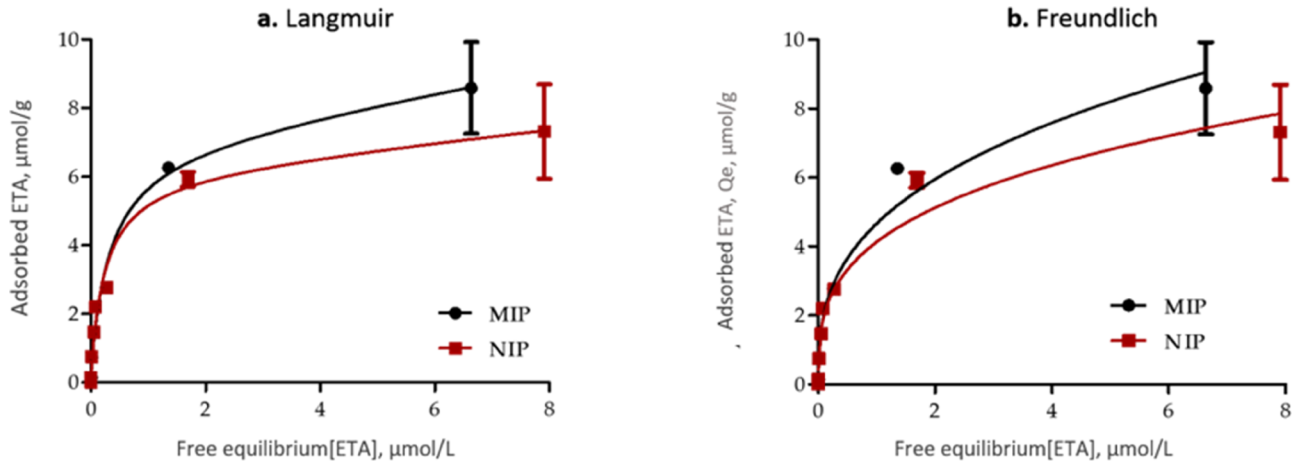

Figure 4. Langmuir (a) and Freundlich (b) isothermal adsorption plot of the adsorbed concentration of ergotamine (ETA, μmol/g) to styrene-based MIP and NIP as a function of the concentration of free ETA at equilibrium. The data in the figure represent mean ± standard error (n = 3)

model, with R^2 greater than 0.95. The Akaike information criterion (AIC) used to identify the best fit model indicated a better fit with the Langmuir (88−97% probability of being correct) compared to Freundlich model (3−12% probability of being correct). For both polymers, the absolute sum of squares was lower with the Langmuir (9.18 and 8.62 for MIP and NIP, respectively) compared to Freundlich model (10.68 and 11.12 for MIP and NIP, respectively).

The Langmuir isothermal adsorption constants (K_L, R_L, and Q_o) and the equations used to determine the constants are presented in Table 2. The R_L values in the present study were found to be between 0.37 and 0.38 for both polymers, indicating a favorable adsorption between ETA and the polymer. However, there was no difference between the polymer types. With regard to the maximum adsorption capacity (Q_o), results showed that Q_o was numerically greater for MIP (8.68 μmol/g) than for NIP (7.55 μmol/g) at pH 6.8 in 0.1 M phosphate buffer at 39 °C. A positive K_L was noticed for both polymers (K_L > 0.37) indicating that the interactions were spontaneous and energetically favorable.

Selectivity Study. Adsorption isotherms in the presence of structurally related alkaloids were used to differentiate the polymers with regard to interaction selectivity. The effect of imprinting on the selectivity of different ergot alkaloids is shown in Figure 5. The adsorption coefficient, selectivity coefficient, and imprinting selectivity data for binding selectivity of polymers toward ergot alkaloids are shown in Table 3. MIP exhibited numerically higher adsorption levels to ETA compared to NIP, and both polymers exhibited similar adsorption to 2-bromo-alpha-ergocryptine (BC). Both polymers had lower affinities toward methylergonovine (ME) and lysergol (LY). There was significant interaction (P < 0.001) between the product and the alkaloid types with respect to adsorption coefficients. There was comparatively greater adsorption of ME and LY for MIP (lower k' values) compared to NIP (k' values of 25 and 50). There was no difference (P = 0.24) between the polymers when alkaloids were grouped as

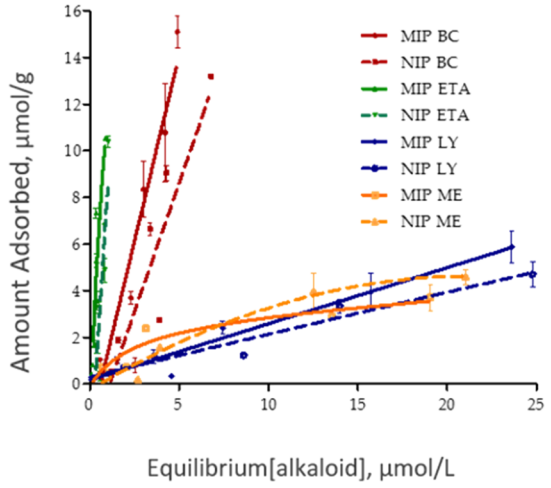

Figure 5. Isothermal competitive adsorption plot using a one-site total binding model for ETA, BC, ME, and LY on the MIP (solid line) and NIP (dotted line) polymer at an inclusion rate of 0.1 mg/mL in the ammonium citrate buffer of pH 6.7. The data in the figure represent mean ± standard error of the mean (n = 3).

https://doi.org/10.1021/acsomega.1c02158
ACS Omega 2021, 6, 30260−30280

Table 3. Adsorption Coefficient (k), Selectivity Coefficient (k'), and Effect of Imprinting (k'') of Styrene-based Molecularly Imprinted (MIP) and Non-imprinted (NIP) Polymers for Different Ergot[a]

	MIP		NIP		imprinting effect
alkaloids	k	k'	k	k'	k''
ergotamine	0.924 ± 0.017[a]		0.910 ± 0.005[a]		
methylergonovine	0.122 ± 0.006[a]	7.590 ± 0.403	0.037 ± 0.003[b]	24.97 ± 1.882	0.308 ± 0.025
2-bromo-α-ergocryptine	0.755 ± 0.006[a]	1.223 ± 0.010	0.750 ± 0.011[a]	1.213 ± 0.018	1.009 ± 0.015
lysergol	0.041 ± 0.003[a]	22.763 ± 0.192	0.018 ± 0.001[a]	50.063 ± 1.360	0.455 ± 0.012

[a]Data represent the mean affinity value ± standard error of mean (n = 3). k: adsorption coefficient; k': selectivity coefficient; k'': effect of imprinting on selectivity. Coefficient values with different superscripts differ (P < 0.01) between MIP and NIP within a given alkaloid. Polymer type x alkaloid type interacted (P < 0.01)

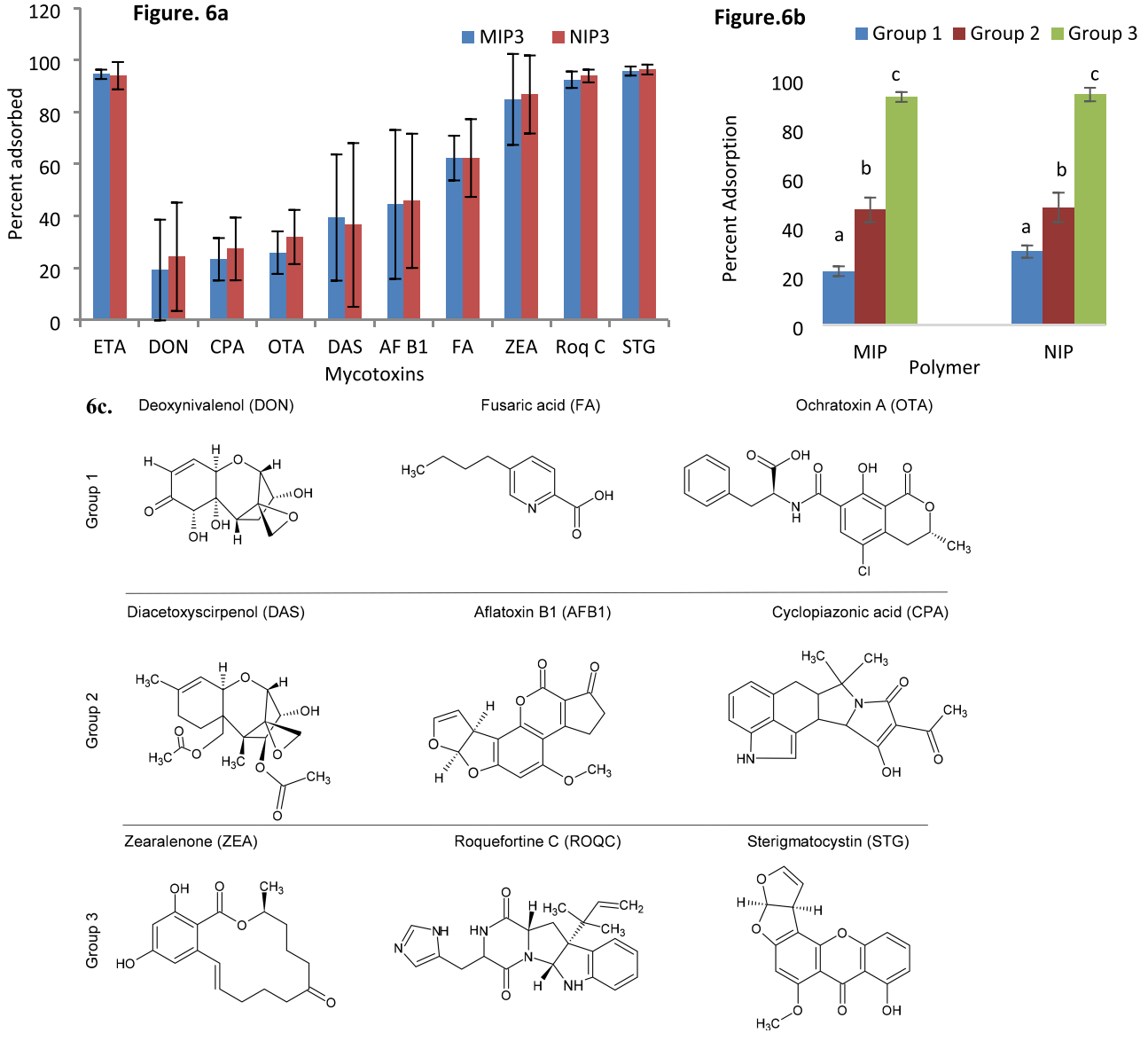

Figure 6. (a) Cross reactivity of ten different mycotoxins toward MIP and NIP (mean ± SEM; n = 3). (b) Adsorption comparison of three groups of mycotoxins based on structure and pKa (mean ± SEM; n = 21); different letters indicate significant differences in adsorption treatment means (ANOVA: P < 0.05). c) Structure of different mycotoxins grouped based on structure and pK_a. Adsorption study was conducted in 0.01 M ammonium citrate buffer media of pH 6.7.

ergopeptines and ergolines (ergopeptines: ETA and BC; ergolines: ME and LY). In reference to the selectivity coefficient (k'), a lower k' value indicates better selectivity of polymer toward rebinding of structurally similar compounds. Comparing k' values between polymers, it was evident that MIP bound structurally related compounds to a greater degree compared to NIP. The k'' is intended to evaluate the imprinting effect, where higher coefficients indicated greater selectivity toward the template. The k'' values were not different from 1 for BC and <1 (Table 3) with respect to the

https://doi.org/10.1021/acsomega.1c02158
ACS Omega 2021, 6, 30260−30280

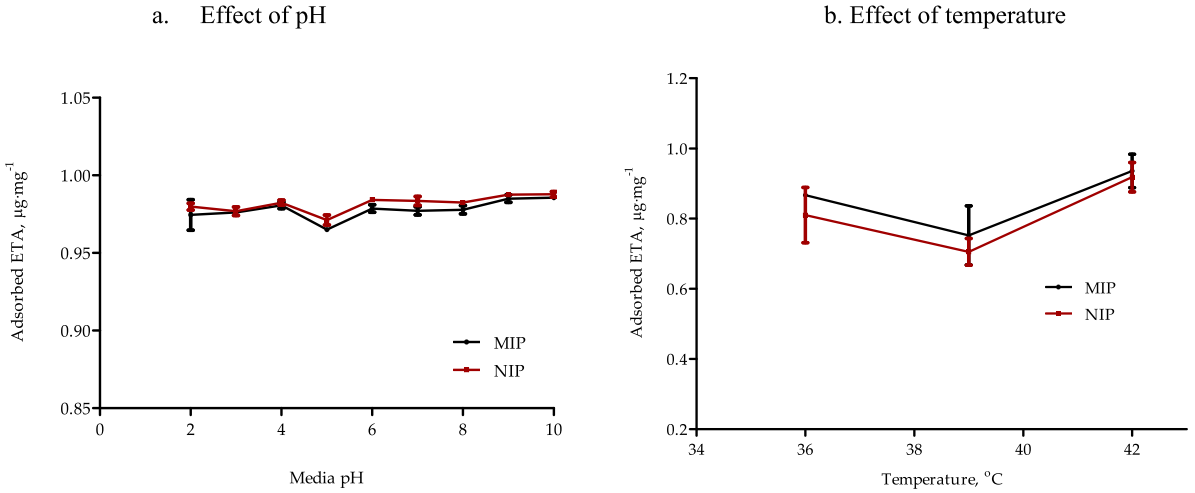

Figure 7. Effect of pH (a) and temperature (b) on the adsorption of ergotamine (ETA, 1 mg/L initial conc.) by molecularly imprinted (MIP) and non-imprinted (NIP) polymers (0.1 mg/mL of polymer inclusion) in 10 mL of the phosphate buffer (0.1 M, pH 6.8). The data in the figure represent mean ± SEM (n = 3).

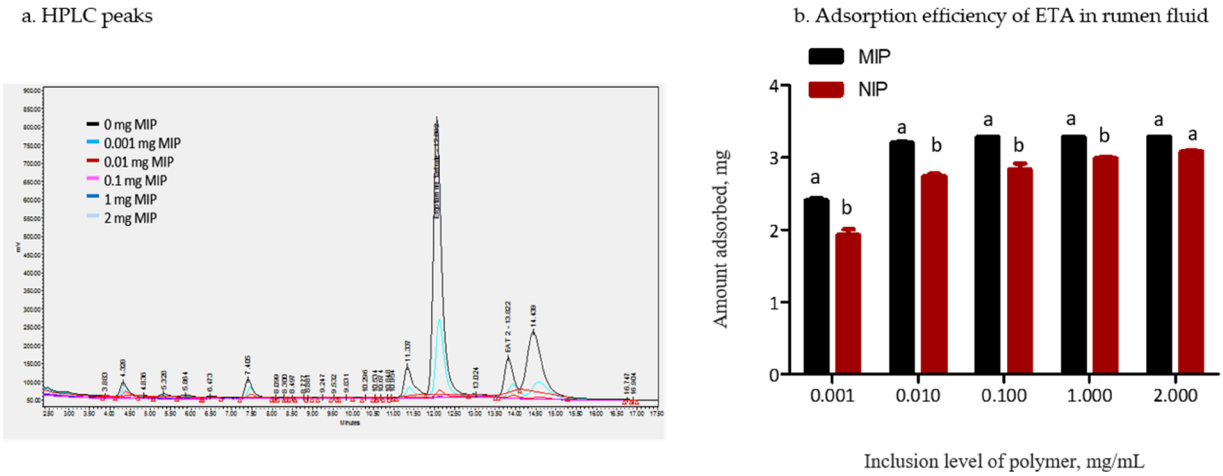

Figure 8. (a) HPLC peaks of samples spiked with ergotamine (ETA, 3.3 mg/L) in rumen fluid dosed with five levels of styrene-based molecularly imprinted (MIP) polymer. (b) Adsorption efficiency of ETA (3.3 mg/L) with increasing levels of molecularly imprinted (MIP) and non-imprinted (NIP) polymers in rumen fluid. The data represent mean ±SEM (n = 3). Means with different letters within the inclusion level differ significantly (P < 0.05).

binding of ME and LY, providing no evidence for imprinting effects.

Cross-Reactivity Experiment. Cross-reactivity was evaluated from the adsorption properties of MIP and NIP to frequently occurring mycotoxins (Figure 6). Different mycotoxins with different functional groups (carboxylic acid and amines), pK_a's (acidic, neutral and basic), and solubilities were selected. Both polymers exhibited nonspecific adsorption to different toxins (Figure 6a) to different degrees, and there was no difference in the mean adsorption between MIP and NIP for any of the mycotoxins. Toxins were grouped according to their structural conformation and functional groups (Figure 6c): the group of toxins with low solubility in water and having basic pK_a's (zearalenone (ZEA), roquefortine C (ROQC), and sterigmatocystin (STG)), the second group that is more hydrophilic in nature with low pK_a's (deoxynivalenol (DON), fusaric acid (FA), and ochratoxin A (OTA)), and the third group that has a tendency to dissolve in water (cyclopiazonic acid (CPA) and Diacetoxyscirpenol (DAS)). The first group of mycotoxins exhibited more than 80% adsorption, while the second group exhibited a low degree of interaction with the polymers. The last group of toxins demonstrated an intermediate degree of adsorption to polymers. The adsorption was significantly different between the three groups of toxins (P < 0.001) (Figure 6b); however, there was no difference between the polymers in adsorbing any of these toxins (P = 0.462).

Effect of pH and Temperature. The effect of pH on the adsorption of ETA to both polymers is shown in Figure 7a. The ETA adsorption ranged between 96 and 99%, and there was no difference across the pH range tested (P = 0.24) or between polymers (P = 0.18). Figure 7b shows the adsorption of ETA when 1 mg of polymer was combined with an initial concentration of 1 mg/L of ETA in 0.01 M phosphate buffer at pH 6.8 at three different temperatures (36, 39, and 42 °C). Even though the data for both polymers indicated that adsorption was reduced by nearly 10% when the temperature was 39 °C, the decrease was not statistically significant (P > 0.11) and there was no difference (P = 0.64) between the polymer types for each temperature tested. There were no pH × polymer interaction (P = 0.64), no temperature × polymer

https://doi.org/10.1021/acsomega.1c02158
ACS Omega 2021, 6, 30260−30280

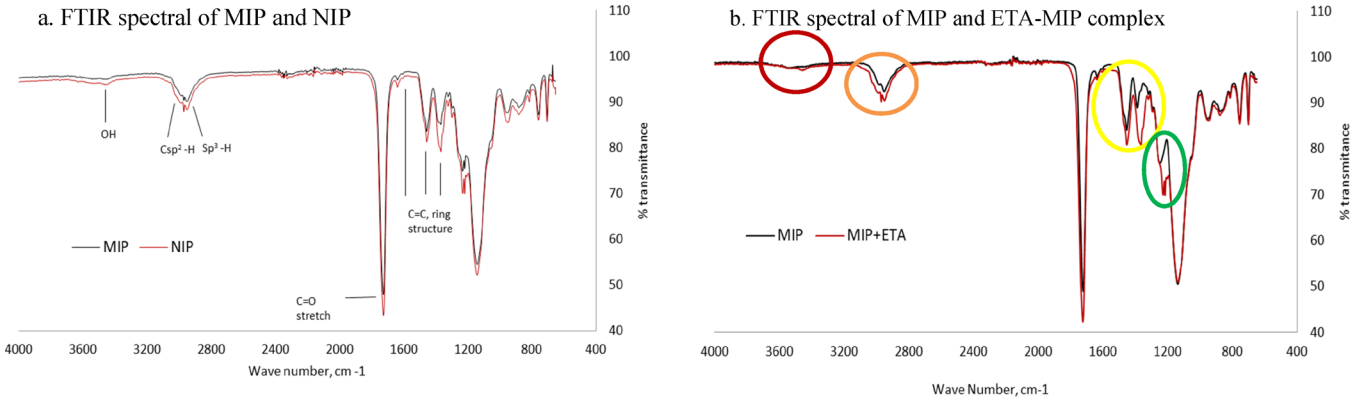

Figure 9. FTIR spectra of (a) comparison between the imprinted (MIP) and non-imprinted (NIP) polymers and (b) between MIP and the [ETA−MIP] complex recorded in the frequency range 4000−650 cm^{-1}.

interaction (P = 0.78), no difference between the polymer types (P > 0.18) or between the mean temperatures (P > 0.11), and no effect of pH on adsorption (P = 0.24).

Adsorption of ETA from the Complex Solution. The adsorption efficiency of different inclusion levels of MIP for ETA in comparison to control (NIP) was determined in ruminal fluid collected from the foregut of the ruminant animal. Comparative chromatograms from samples spiked with 3.3 mg/L ETA in rumen fluid that were dosed with increasing levels of MIP are shown in Figure 8a. With the increasing dose of polymer in rumen fluid, the peak area of ETA decreased. Maximum adsorption was noticed at 0.01% w/v (100 mg/L) with maximum efficiency of 97% for MIP and 85% for NIP (Figure 8b). There was minimal increase in adsorption with further increase of polymer inclusion rates, indicating an optimum (reaching 97%) at 0.01% w/v of the polymer for the adsorption of 3.3 mg/L of ETA from rumen fluid. However, at similar inclusion rates, NIP exhibited significantly (P < 0.01) lower adsorption. There was no interaction (P = 0.23) between the inclusion rate and polymer type, and the mean adsorption of the NIP was almost 10 percentage points lower than that of MIP.

Fourier Transform Infrared (FTIR). Spectrum comparison between MIP and NIP (Figure 9a) and between MIP and the [MIP + ETA] complex (Figure 9b) over the frequency range of 4000−650 cm^{-1} was conducted to differentiate the polymers and functional groups involved in interaction with the template, respectively. Absorption peaks for C═C, typical for the ring structure of styrene, were observed at 1600, 1494, and 1449 cm^{-1}, and the presence of sp^2 hybridization in the styrene ring system was evident from the absorption spectrum below 3000 cm^{-1}. A broad absorption band for the hydroxyl group of HEMA was found at 3430 cm^{-1}.

Both polymers had similar IR spectra indicating expected similarity in the functional groups present (Figure 9a), suggesting the preservation of these same functional groups after the solvent-based removal of the template from the MIP. The results also indicated minimum covalent bonds between the template and the polymer. The C═O band at 1729 cm^{-1} from NIP was of similar intensity compared to MIP, showing a similar backbone structure. Some of the characteristic bands of both polymers included −CH3 (asymmetry) at 2955 cm^{-1}, carbonyl stretch (−C═O) at 1724 cm^{-1}, −C−C− at 1635−1670 cm^{-1}, −CH3 (symmetry) at 1450 cm^{-1}, −C−O or −C−O−C− stretch at 1250 cm^{-1}, and C−H vibrations at 756 and 1388 cm^{-1}.

Figure 9b represents FTIR spectra of MIP before and after exposure to ETA in 0.1 mol/L phosphate buffer at pH 6.8. The [MIP + ETA] complex was washed with deionized water to remove free ETA and later freeze-dried before analysis. The [MIP + ETA] complex showed all characteristic bands to that of the MIP polymer; however, there were changes in the bands' intensity at 3400 cm^{-1} (red), between 2950 and 2970 cm^{-1} (orange), at 1350 cm^{-1} (yellow), and at 1260 cm^{-1} (green) due to the stretching in the hydrogen bond (O−H, C−H, or the N−H), presence of ring structures, change in C═C stretching, and change in single bond stretch (C−N and C−O), respectively.

Molecular Mechanics Docking Prediction between the Polymer and Template and Comparison with Other Commonly Used Monomeric Types Used in MIP Production. A screening was performed comparing the docking affinity of 29 different monomers comprising styrene and HEMA used in the herein study to other commonly used monomers in the production of MIP/NIP[24] by means of *in silico* computational techniques. Noncharged ETA and the protonated form of ETA (ETA+) bearing a positive charge on the aromatic nitrogen of the ergoline moiety were evaluated as ligands. The uncharged ETA was evaluated as the major species up to pH 7.8, with ETA-NH+ being represented between 1 and 60% between pH 6 and 8 and further becoming the major species when reaching pH 9.7. Table 4 reports the best affinity based on the lowest attainable docking energy (kcal/mol) and overall average affinity out of the nine best positions for the different tested monomers. Aromatic-based, such as vinyl-benzenes, vinyl-benzoic acid, ethoxy-hydroxy mandelic acid, and styrene, monomers exhibited the highest affinity (>−4.6 kcal/mol) to ETA and ETA+; most of the methacrylate-based monomers had lesser affinities (−1.2 to −3.5 kcal/mol) or could be affected by the charge of ETA, which demonstrated the importance of the ETA heterocycle in establishing the interaction and multiple $\pi-\pi$ static effects associated with the docking to benzene rings. The affinity of methacrylate-based monomers was even lessened for ETA+ (i.e., methylmethacrylate, affinity of −5.1 vs −1.8 kcal/mol for ETA and ETA+, respectively), further making monomers carrying benzene ring, the composition of choice for interacting with the investigated ergot alkaloid. The evaluation of the docking affinity between polymeric chains of 10 monomeric unit length was carried out and showed that, again, polystyrene had the highest affinity (−8.6 kcal/mol) compared to polyacrylate polymers independently from the

https://doi.org/10.1021/acsomega.1c02158
ACS Omega 2021, 6, 30260−30280

Table 4. Interaction Affinity of Ergotamine (Unprotonated (ETA) and Singly Protonated (ETA+) States) to Monomers, Polymer Chains (10 U), and Large Polymeric Material Used in the Production of Imprinted Polymers Compared to the Formulation Used in This Study by Means of Molecular Mechanics

			docking affinity (kcal/mol)[a]			
			ETA		ETA+	
monomer unit	abbr.	free energy[b] (kJ/mol)	best	average	best	average
ethoxyhydroxymandelic acid	EHMA	58.9	−5.6	−5.4 ± 0.1	−4.3	−4.0 ± 0.1
1-2-vinyl benzene	VB	39.2	−5.3	−5.0 ± 0.3	−5.2	−4.8 ± 0.2
4-vinyl benzoic acid	VBA	23.0	−5.3	−4.8 ± 0.2	−5.3	−4.9 ± 0.2
methylmethacrylate	MMA	89.9	−5.3	−5.0 ± 0.1	−1.8	−1.6 ± 0.1
trifluoromethylacrylic acid	TFMAA	−44.1	−5.3	−4.7 ± 0.2	−5.3	−4.9 ± 0.1
1-3-vinyl benzene	VB	19.9	−4.9	−4.4 ± 0.3	−4.8	−4.2 ± 0.3
methylhydroxymethacrylate	MHMA	76.0	−4.8	−4.5 ± 0.1	−4.7	−4.3 ± 0.2
1-4-vinyl benzene	VB	19.9	−4.7	−4.5 ± 0.1	−4.5	−4.3 ± 0.2
styrene	STY	18.1	−4.6	−4.2 ± 0.1	−4.6	−4.2 ± 0.2
dimethylacrylamide	DMA	−24.9	−3.9	−3.4 ± 0.1	−2.9	−2.7 ± 0.1
4-vinyl pyridine	VP	14.2	−3.8	−3.6 ± 0.1	−4.1	−3.8 ± 0.1
2-vinyl pyridine	VP	17.0	−3.7	−3.4 ± 0.1	−3.6	−3.4 ± 0.1
pentaerythrityl triacrylate	PETA	36.4	−3.7	−3.5 ± 0.1	−2.9	−2.7 ± 0.1
trimethylolpropane trimethacrylate	TMPTMA	17.0	−3.5	−3.0 ± 0.2	−3.5	−3.1 ± 0.1
2-acrylamido-2-methyl-1-propane sulfonic acid	AMPSA	−58.2	−3.4	−3.0 ± 0.2	−2.6	−2.3 ± 0.1
ethylene glycol dimethacrylate	EGDMA	13.3	−3.1	−2.7 ± 0.1	−3.3	−2.9 ± 0.2
hydroxyethyl methacrylate	HEMA	7.4	−2.8	−2.6 ± 0.1	−2.8	−2.5 ± 0.1
propyl acrylate	PA	−23.8	−2.7	−2.5 ± 0.1	−2.8	−2.6 ± 0.1
dimethylaminoethyl methacrylate	DMAEM	15.9	−2.0	−1.8 ± 0.0	−2.6	−2.3 ± 0.1
methylmethacrylate	MMA	−14.5	−1.9	−1.7 ± 0.1	−1.8	−1.6 ± 0.1
vinyl pyrrolidone	VPone	−28.9	−1.9	−1.7 ± 0.0	−1.8	−1.6 ± 0.0
methacrylamide	MA	−29.5	−1.8	−1.6 ± 0.1	−3.0	−2.8 ± 0.0
methyl acrylate	MA	−21.2	−1.8	−1.5 ± 0.1	−1.7	−1.5 ± 0.0
acrylic acid	AA	−33.3	−1.7	−1.5 ± 0.0	−1.7	−1.6 ± 0.0
1-vinyl imidazole	VI	210.5	−1.6	−1.4 ± 0.1	−1.6	−1.4 ± 0.1
acrylamide	A	−29.2	−1.4	−1.3 ± 0.1	−1.7	−1.5 ± 0.0
propylene	PP	−4.9	−1.2	−1.1 ± 0.0	−1.2	−1.1 ± 0.0
vinyl alcohol	VA	−1.5	−1.2	−1.1 ± 0.0	−1.2	−1.0 ± 0.1
vinyl fluoride	VF	−2.4	−1.2	−1.0 ± 0.0	−1.1	−1.0 ± 0.0
polymer chain						
MIP polymer: styrene-methylmethacrylate, 100 Å[c]	-[PMMA-PS-PMA-PMAA]n		−11.7	−10.8 ± 0.3	−11.1	−9.9 ± 0.5
NIP polymer: styrene-methylmethacrylate, 100 Å[d]	-[PMMA-PS-PMA-PMAA]n		−10.4	−9.6 ± 0.4	−10.0	−9.6 ± 0.2
MIP/NIP Chain, 10 U (Units)	-[EGDMA2-STY2-HEMA]2	188.9	−9.2	−8.5 ± 0.3	−9.3	−8.6 ± 0.3
polystyrene (atactic), 10 U	aPSYN10	2057.0	−8.6	−8.0 ± 0.2	−8.6	−7.9 ± 0.3
polypropyl acrylate (atactic), 10 U	aPPA10	−124.1	−7.2	−6.6 ± 0.2	−7.2	−6.5 ± 0.3
polystyrene (syndio), 10 U	sPSTY	238.9	−6.5	−6.3 ± 0.1	−6.2	−6.1 ± 0.1
polymethyl methacrylate (atactic), 10 U	aPMMA10	121.2	−6.3	−5.8 ± 0.3	−6.3	−5.8 ± 0.3
polymethyl methacrylate (syndio)	sMMA	123.5	−6.1	−5.7 ± 0.1	−6.0	−5.7 ± 0.1
polymethylacrylate (atactic), 10 U	aPMA10	−86.2	−5.8	−5.4 ± 0.2	−5.8	−5.5 ± 0.2
polyvinyl pyrrolidone (atactic), 10 U	aPVP10	198.1	−5.6	−5.2 ± 0.2	−5.8	−5.2 ± 0.3
polyhydroxyethyl methacrylate (atactic), 10 U	aPHEMA	151.2	−5.6	−5.3 ± 0.1	−5.2	−4.6 ± 0.2
polypropylene (atactic), 10 U	aPPE10	74.6	−5.3	−5.1 ± 0.1	−5.4	−5.1 ± 0.1
polymethylmethacrylate (isotactic), 10 U	iPMMA	123.4	−5.1	−4.7 ± 0.2	−5.1	−4.7 ± 0.2
polyacrylic acid (atactic), 10 U	aPAA10	−260.4	−4.8	−4.4 ± 0.2	−4.7	−4.3 ± 0.2
polyvinyl fluoride (atactic), 10 U	aPVF10	−34.2	−4.6	−4.3 ± 0.2	−4.7	−4.3 ± 0.2
polyvinyl alcohol (atactic), 10 U	aPVA10	50.2	−3.9	−3.7 ± 0.1	−4.0	−3.8 ± 0.0
polyamide (atactic), 10 U	aPA10	−133.0	−2.6	−2.4 ± 0.0	−2.8	−2.7 ± 0.0

[a]Docking experiments and affinity measurements were performed with AutoDock Vina. [b]Minimization of all other monomers and ETA was performed under MMFF94 force field after 100,000 minimization iterations. [c]MIP built and equilibrated at 338 K (CHARMM-GUI, CHARMM36 all atom force field) by dynamic simulation in a toluene cubical solvent box of 100 Å side length with a volumic ratio of 87.7% corresponding to the MIP occupancy compared to NIP using pore diameter information (Table 1). [d]NIP built and equilibrated at 338 K (CHARMM-GUI) by dynamic simulation in a toluene cubical solvent box of 100 Å side length with a volumic ratio of 100% corresponding to the NIP occupancy.

ETA charge state. Combining styrene and HEMA in a co-polymer cross-linked with EGDMA further increased the docking affinity stability (−9.2 kcal/mol). Finally, the same composition was placed in a toluene solvent cubical box of 100 Å side length to achieve a volumetric ratio of 87.7 and 100% for, respectively, MIP and NIP, corresponding to the

https://doi.org/10.1021/acsomega.1c02158
ACS Omega 2021, 6, 30260−30280

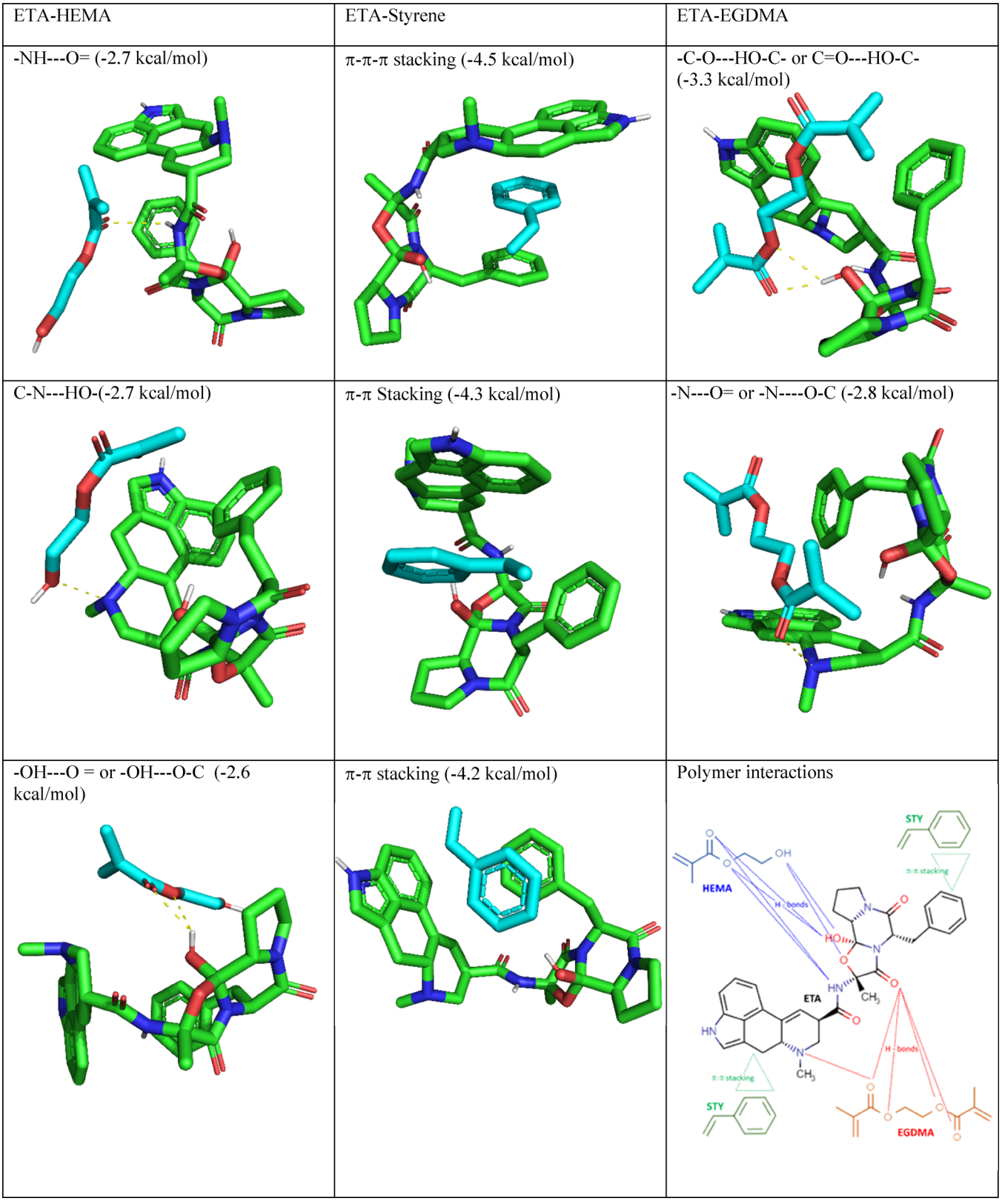

Figure 10. Computer-generated views of the energy-minimized docking of ergotamine (ETA, in green) to various monomers (styrene, HEMA, and EGDMA; in blue) used in the composition of molecularly imprinted polymers using AutoDock Vina. The highest energy favorable interaction was measured as the lowest affinity energy reported in kcal/mol.

pore volume differences reported in Table 1. The affinity was further denoted for MIP over NIP, at −11.7 and −10.4 kcal/mol, respectively. A slightly lower affinity overall was seen for the ETA+ state, −11.1 and −10.0 kcal/mol. For the monomers and 10-unit polymer chains, only marginal differences between those two states were found.

https://doi.org/10.1021/acsomega.1c02158
ACS Omega 2021, 6, 30260−30280

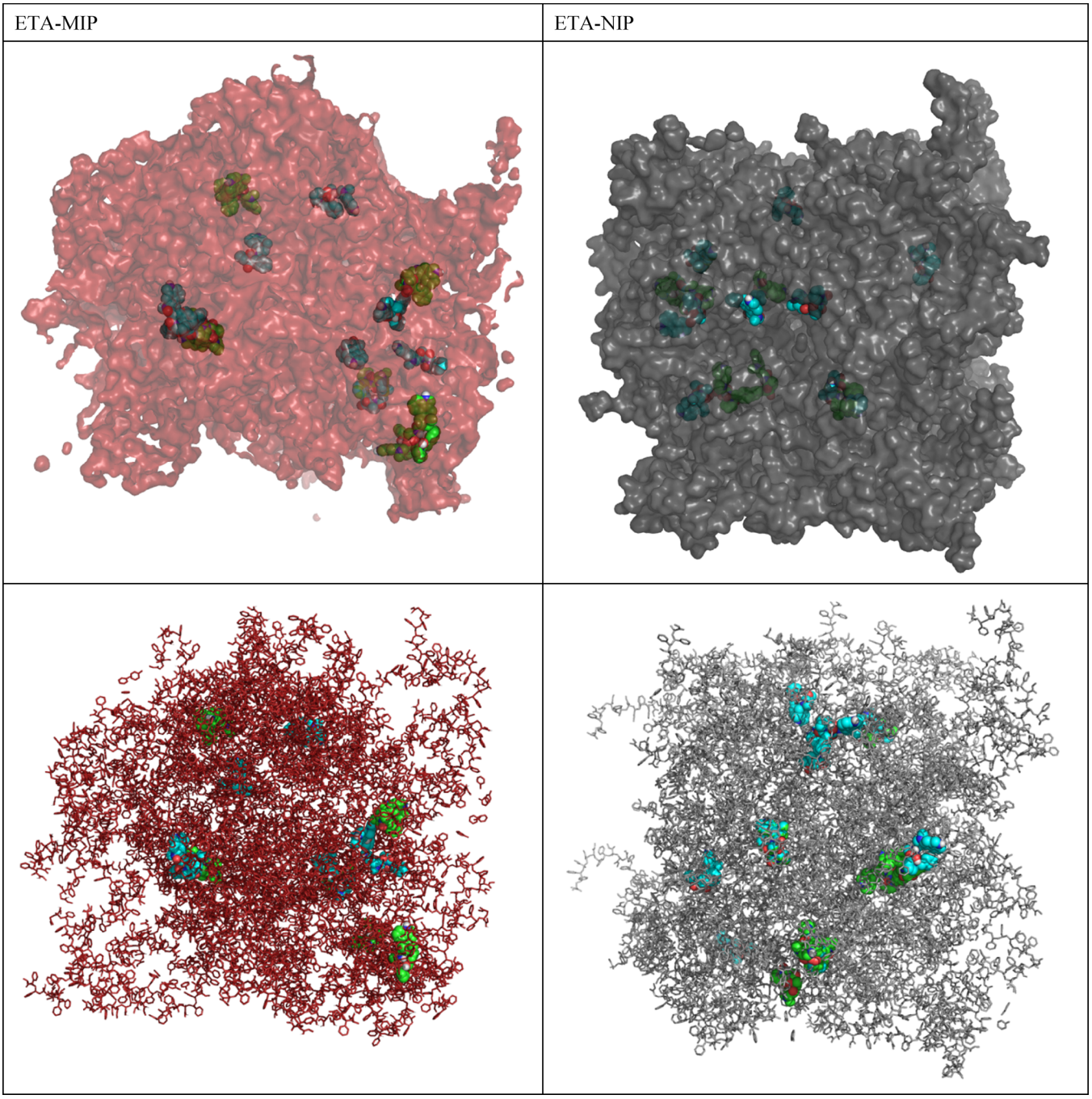

Figure 11. Computer-generated views of the energy-minimized docking of ergotamine (ETA, in green; ETA+, in blue) to styrene-based molecularly imprinted (MIP, in red) and non-imprinted (NIP, in gray) polymers structures generated with acrylate and styrene-base monomers and equilibrated in a toluene solvent cubical box of 100 Å side length at 338 K and further interacted with ETA.

From the computational work performed herein, several possible interactions between the monomer and the template were characterized (Figure 10). Interactions involved the hydrogen bond between the hydrogen atom of hydroxyethyl-methacrylate or the ethylene glycol dimethacrylate and nitrogen or the oxygen atom of the ETA. A $\pi-\pi-\pi$ interaction between the multiple aromatic rings of ergotamine that could organize around the benzene ring of styrene monomers was characterized. Another interaction could result from the hydrophobic attraction between the polymer and the alkaloids due to their hydrophobic nature. Finally, the cavities created in the polymer during the imprinting process could create a structural complimentary void that allows structural recognition during the rebinding process. Modelization of the bulk MIP and NIP polymers according to the pore volume and associated volumetric ratio of MIP over NIP (87.7%) showed that the final MIP polymer, as expected, had larger cavities that could facilitate the ETA penetration further inside the core MIP macromolecular structure, whereas ETA tended to be localized at the periphery with the NIP (Figure 11).

DISCUSSION

An important challenge in understanding ergot alkaloid toxicity is the highly variable individual animal response to exposure.[25]

https://doi.org/10.1021/acsomega.1c02158
ACS Omega 2021, 6, 30260−30280

This disparity in toxicity could be due to the changing proportions or distribution of alkaloids, change in alkaloid concentration, and/or isomerization of alkaloids in the rumen due to the microbial enzymatic metabolism and the ruminal physiological conditions.[26,27] Therefore, it is very important to use an adsorbent material that could effectively interact with alkaloids and offer means to separate those contaminants either for isolation−concentration−quantification purposes or for attempting to reduce their bioavailability and mitigating their impact. The success in developing analytical methods for the extraction and identification of trace levels of different naturally occurring alkaloids as well as their digestive metabolites is intricately linked to better extraction techniques specifically suited to ameliorate their isolation from complex matrices such as the ruminal environment. Therefore, highly specialized and efficient adsorbents, specifically molecularly imprinted polymers, working on the basis of molecular recognition principles have been synthesized and studied.

Optimizing polymer synthesis with an efficient imprinting process plays a critical role in molecular recognition properties of MIPs.[28] Noncovalent interactions including ionic, hydrophobic, and hydrogen bonding between the template and the functional monomers[29,30] drive the imprinting processes that later maintain molecular recognition properties when the template is removed from the then ″imprinted″ polymers. Synthesis of high-affinity MIPs utilizing noncovalent interactions[31,32] between monomers and template has been well documented by means of free radical polymerization followed by co-polymerization with a cross-linker[33,34] under optimized pre-polymerization conditions.[35,36] Spatial arrangements of shape selective cavities during the interactions between complementary functional groups of the template and the monomers are the driving force behind the binding selectivity of MIP.[37] In the present study, ETA was used as a template molecule that represents the ergo-peptide family, which has well-established analytical methods for its quantification.[38−40] The ergoline structure and side chain tripeptide in ETA provide different functional groups capable of forming complementary interactions with functional monomers (e.g., styrene and HEMA). The ergoline portion of the ETA molecule includes one basic, tertiary amino group; one strongly polar heterocyclic, pyrrole ring; one amide group; and several low-polarity hydrocarbon fragments (e.g., benzene ring and double bond) that can interact with monomers and cross-linker. At pH 6.8, which was the condition used for adsorption kinetic studies, more than half of the ETA molecules (nearly 70%) are singly charged and may contribute to interaction with complimentary functional groups in the MIP, mainly the hydroxyl groups. The hydroxyl group of HEMA simultaneously functions as a hydrogen donor as well as a hydrogen acceptor, whereas styrene acts as an electron-rich π donor that could be involved in $\pi-\pi$ stacking interaction with the aromatic ring members of the ergot alkaloid, which was confirmed by means of *in silico* molecular mechanics further accounting for $\pi-\pi-\pi$ interaction, and the largest affinity of interaction among 29 screened monomers.

Studies have shown weak $\pi-\pi$ stacking interactions between aromatic groups involving phenol and ethylbenzene[41] and aromatic rings of biomolecules that are involved in stabilizing ligands into macromolecules.[42] Additionally, the carbonyl and alcohol groups in ETA enable a range of noncovalent electrostatic interactions during pre-polymerization that are conducive to the formation of stable interactions between the template and polymer during the polymerization process and consequent highly porous polymers post template removal. A strong interaction between the template and the monomers is generally considered favorable to the production of high-affinity binding sites within the MIPs. However, this may cause a ″template bleeding phenomenon″ during MIP utilization.

″Template bleeding″ is a phenomenon of slow release of the template in small quantities coming from leakage of a physically entrapped template facilitated by the swelling and shrinkage of the polymer material, or formation of template clusters that could be released by the polymeric material.[18,43] Generally, for low-molecular-weight templates, highly cross-linked polymers are used to ensure preservation of the imprint cavity after its removal. Conversely, for a larger template, high cross-link densities can affect the mass transfer of the template, affect rebinding kinetics, and lead to slow template removal and thorough washing setps[44,45] or even permanent entrapment in the polymer network.[46] Even though advanced techniques like thermal annealing, microwave-assisted extraction, Soxhlet extraction, and super critical fluid template desorption[43,47] have been used to recover the template from imprinted polymer, complete removal of template is often not possible.

In the present study, quantitatively, most template removal occurred with the use of five consecutive methanol washes in a time-dependent fashion. The recovery of the template was facilitated by high ETA solubility in the organic solvent, especially a protic organic solvent like methanol. Additionally, methanol can penetrate the polymer and compete with and displace noncovalent bonding. In general, noncovalent interactions are attenuated using mild acidic or basic organic solvents that facilitate the removal of the template from the polymerized network. Organic solvents containing acid or base additives that solubilize the template are used when electrostatic force, hydrophobic interaction, or hydrogen bonding is involved, especially with biomolecular templates (e.g., lysozyme and cytochrome).[47,48] Effective template removal can be achieved for molecules with a low molecular weight (<1500 Da).[45,50−52] Harsher methods are not recommended as they do not guarantee complete template removal[48,53,54] and may ultimately affect the final polymeric network structure, with loss of affinity and/or specificity in rebinding.[54] In one of the earlier studies, a total recovery of 67−88% was reported when co-polymers of methacrylic acid and 2-hydroxyethyl methacrylate were imprinted with theophylline and extracted with acidic methanol.[55] In the present study, even though ETA could be defined as a small molecule (581.673 g/mol), the presence of key functional groups (carbonyl, hydroxyl, amide, and benzyl) can possibly interact via ionic, hydrophobic, $\pi-\pi$, and electrostatic interactions, along with hydrogen bonding. The multiplicity of these interactions, as confirmed through computational modeling, could explain the slower template release and also the longer immobilization into the polymer matrix.

Template bleeding is also controlled by the integrity of the polymer that is dependent on the composition of functional monomers and polymerization technique.[56] The monomer to cross-linker ratio of 3:10 (molar basis) was chosen in this study based on binding selectivity criteria observed for three different ratios of monomer/cross-linker (3:2.5, 3:5, and 3:10) tested in a preliminary study (data not shown). The highest ratio of 3:10 showed more than 95% adsorption compared to lower ratios. Similar observations were made in other studies that

https://doi.org/10.1021/acsomega.1c02158
ACS Omega 2021, 6, 30260−30280

aimed at screening different ratios of aromatic template and functional monomers.[57] Furthermore, suspension polymerized imprinted beads using methacrylate and EGDMA as monomer and cross-linker in a ratio of 1:4, respectively, exhibited superior binding affinity and selectivity toward ergot alkaloids when metergoline was used as the template.[17] The production of a copolymer in the present study correlates with our experimental and predictive evaluations. The use of a co-polymer with acrylate and styrene-based material enhanced further the sorption capabilities of both MIP and NIP produced. Usually, along with the composition of functional monomers, the polymerization techniques used for the synthesis of polymers regulate the structural characteristics of the end product. The range of particle size distribution is a function of monomer to polymer conversion, chain length propagation, and rate of chain length termination during polymerization as described by the power law.[58]

The polymers synthesized in the present study were mesoporous in nature. The increase in volume of N_2 adsorbed with the increase in relative pressure observed in nitrogen sorption porosimetry could be attributed to the capillary condensation of nitrogen into pores of the polymer. The comparatively large BET surface area and pore volume of MIP were presumably created when the imprinting template molecule was removed from the polymer. Additionally, with bulk polymerization, the swelling properties in different solvents may have contributed to the wide range of particle size distribution from 5 to 90 μm. In deionized water, a slight aggregation was noticed indicating interparticulate hydrophobic interactions between the polymer molecules yielding a nondistinct continuous particle size distribution. These observations were confirmed with the SEM micrograph that revealed non-uniform particles with irregular morphologies for MIPs. The surface of NIP was more regular than the surface of MIP, the latter exhibiting more cavities induced by ETA imprinting, suggesting changes in its structural organization. Furthermore, the polymers were amorphous in nature, which is typical for free radical polymerization with concentrated solutions of monomers and high levels of cross-linkers. The amorphous nature of the MIP and NIP synthesized using free radical polymerizations was also observed in other studies using X-ray diffraction.[59,60] Such polymers have been shown to have numerous non-uniform distributions of binding sites producing nonlinear binding isotherms[61,62] that could be described using established Langmuir and Freundlich regressions.

Langmuir adsorption isotherms quantitatively describe monolayer adsorption between solids and liquids and assume identical adsorption sites of uniform energies. The model holds well when there are a finite number of adsorption sites on the outer surface of an adsorbent and no transmigration of adsorbate on the plane of the surface.[63−65] On the other hand, Freundlich isotherms describe surface adsorption on the adsorbent with multiple layers of adsorption.[66]

Studies have shown that adsorbents with heterogeneous binding sites usually show good fit with nonlinear models like Langmuir and Freundlich.[61,67] In the present study, the Langmuir model provided a better fit than the Freundlich model, with R^2 greater than 0.95. The AICc, a measure comparing validity within a cohort of nonlinear models and frequently used for model selection,[68] indicated a better fit with the Langmuir compared to Freundlich model. Thus, the isotherm study suggested that ergot alkaloid molecules bound to the surface of the polymer with a low propensity to dissociate from that surface and were bound in a single layer to essentially equivalent sites (homogeneous) on the surface of the solid.

The important features of Langmuir isotherms are the adsorption constants K_L, R_L, and Q_o. The K_L refers to binding site affinity, a factor that relates to heat of adsorption.[69] The affinity of adsorption depends on the activity coefficient of occupied and unoccupied sites on the adsorbents at equilibrium,[70] which relates to the molar concentrations of adsorbate in the media. A positive K_L indicates that the interactions are spontaneous and energetically favorable,[71] which was noticed for both polymers ($K_L > 0.37$) in our study. In addition, affinity between the sorbent and sorbate is described only when the adsorption is at equilibrium state. Polymer geometry, polymer hydration, cross-link density, template size, and temperature play an important role in the time needed for large molecular templates to diffuse into the polymer matrix to reach equilibrium.[72,73] A substantial part of the literature investigating rebinding studies confirms an imprinting effect but lacks convincing data on reaching the equilibrium state, especially with large molecule templates such as ETA. Even though some studies have adjusted the incubation period to account for equilibrium in rebinding studies,[74,75] most researchers have used shorter incubation periods without reaching equilibrium either to compare different polymers for adsorption properties or to match the limits of application of the finished polymer products.[76−79] Even though adsorption desorption was noticed up to 14 days (found while washing MIPs to determine template bleeding), all our isothermal adsorption studies were conducted for 90 min, beyond which there was minimal change in equilibrium.

The type of interaction and adsorption affinity between the imprinted polymer and template would vary depending on the properties of interacting medium.[80] Hydrogen bonding greatly contributes to the affinity of MIPs for low-molecular-weight compounds especially in organic or aprotic solvents, and these interactions are generally hampered in aqueous media. In contrast to the few strong bonds that are responsible for the selective interaction between small molecular template and polymer in aprotic organic solvents, multiple weak interactions between the large molecules and the polymer network are ideal for the generation of a strong binding in an aqueous environment.[49,81] Electrostatic interactions seem to play a primary role in recognition if the selectivity is not altered by varying the water concentration of the binding media. Conversely, with hydrogen bonding, the interaction between the polymer and template can be suppressed by increasing the concentration of the compound that has a higher hydrogen bonding capacity (e.g., methanol or water) in the binding media. In addition, it is well known that the diffusion kinetics of large template in a highly cross-linked polymer matrix are a function of its molecular weight, with slow diffusion coefficients for large molecules.[52,82] All our rebinding studies were conducted in aqueous buffer media, thus suggesting that the interaction between ergolines and polymers may have occurred predominantly through hydrophobic interactions.

Separation factor R_L is another constant that is calculated from the Langmuir constant (K_L). The constant R_L is a dimensionless constant that indicates favorability of adsorption.[83] An R_L value between 0 and 1 signifies favorable adsorption, and $R_L > 1$, $R_L = 1$, and $R_L = 0$ indicate unfavorable, linear, and irreversible adsorption, respec-

https://doi.org/10.1021/acsomega.1c02158
ACS Omega 2021, 6, 30260−30280

tively.[71,84] The R_L value in the present study was between 0.37 and 0.38 for both polymers, indicating that the adsorption between ETA and polymer was favorable. However, there was no difference between the polymer types. In addition, the Langmuir constant Q_o obtained from the Langmuir isotherm represents the practical limiting adsorption capacity and is useful in comparing the performance of different adsorbents. It correlates well with specific surface area,[85] and it relates directly with the amount of adsorbate bound from the solution. In the present study, higher adsorption capacity for MIP was observed likely due to large complementary cavities of the template and larger surface area created by the imprinting process.

To determine the selectivity and cross-reactivity of imprinted polymer for various compounds, adsorption isotherms of MIP vs NIP in the presence of structurally related alkaloids and other contaminants were evaluated. Ergotamine has a weak acidic hydroxyl group and an amide moiety that provide unique functional groups necessary for specific interactions with the polymer during imprinting. In addition, $\pi-\pi$ interactions between the tetracyclic ring structure of ETA and styrene may enhance the interaction between the template and polymer. In this study, considering selectivity, both polymers exhibited similar adsorption coefficients (k) to ETA and BC, with lower affinities toward ME and LY, and no differentiation between ergopeptines and ergolines (ergopeptines: ETA and BC; ergolines: ME and LY). Similar results were obtained for selectivity to phenolic compounds, where minimal differences between MIP and NIP were noticed when hydrophobic interactions were involved.[86] These suggest that interaction with alkaloids on the product surface via hydrophobic interaction or π-stacking was common between the MIP and NIP, thereby yielding minimal difference between products.

For evaluation of cross-reactivity, the adsorption properties of MIP and NIP to different mycotoxins with different functional groups (carboxylic acid and amines), pK_a's (acidic, neutral, and basic), and solubilities were determined. Both polymers exhibited nonspecific adsorption to different toxins of variable degrees, and there was no difference in mean adsorption between MIP and NIP for any of the mycotoxins. The group of toxins with low solubility in water and having basic pK_a's is either neutral or positively charged in the adsorption medium of pH 6.8. These molecules (ZEA, RocQ, and STG) are polycyclic, have the possibility of exhibiting hydrophobic interactions, and showed higher adsorption (approximately 85%) compared to the second group of toxins (approximately 30%; DON, FA, and OTA) that are hydrophilic in nature to some extent. The second group of toxins has low pK_a values and exhibited a low degree of interaction with polymers. The last group of toxins included polycyclic compounds (aflatoxin B1 (AFB1) cyclopiazonic acid (CPA)) that had a slightly lower tendency to dissolve in water. This group of toxins exhibited an intermediate degree of adsorption (approximately 50%) to polymers that could be due to hydrophobic interactions. Even though the polymers showed cross-reactivity with different types of toxins, evaluating the adsorption efficacy of the polymers in complex media that vary in pH and temperature and in the presence of interfering compounds is essential to determine their ultimate applicability.

Most of the contaminated feeds including fescue seeds and fescue grass or its products like haylage have a pH range between 3.5 and 8.0, and the ruminal pH of animals grazing fescue would generally be between 6.2 and 6.8. Therefore, it is very important that the adsorption efficacy of the polymers is maintained in a wide range of pH for application of MIP as an extraction material or as a feed toxin adsorbent. Additionally, pH determines the degree of ionization of ETA and dictates its speciation in the solution. The pK_a of the polymer in the adsorption media and the surface charge that can be influenced by the solution pH have been shown to affect its adsorption properties.[87] Under physiological conditions, the pK_a of polymers made from acrylates including polymethylacrylic acid[88] and polyacrylic acid[89] was shown to be nearly 5.0 and 4.3, respectively. In a strongly acidic solution with low pHs, the ETA molecules will be positively charged by the −NH groups' protonation, while the polymer carboxylic functional groups (of HEMA and EGDMA) will also be positively charged due to the protonation of either the carbonyl oxygen or the hydroxyl oxygen. By increasing the pH, the protonation degrees of both ETA molecules and the adsorbent carboxylic groups will significantly be reduced, which may give a chance for proton transfer and interaction via ionic bonding. In the present study, the adsorption efficiency remained similar at pH ranges between 2 and 10 for both polymers. The lack of effect of pH on the adsorption is suggestive of non-ionic interactions, especially hydrophobic interactions being the primary driving force for the adsorption. Additionally, results indicate that pH effects would not limit the utility of the polymers as an extraction material for ergot alkaloids or as an adsorbent in the feed to reduce the bioavailability of ergot alkaloids.

Concerning the effect of temperature, polymers have an innate tendency to swell or collapse with a change in temperature, causing changes in surface properties.[90,91] Generally, chemisorption increases by increasing the temperature due to an increase in the rate of a chemical reaction or by chemically changing the adsorbent and its adsorption sites and activity. The better adsorption at higher temperatures might also indicate the endothermic nature of this process. In addition, if the process is physical adsorption, then the higher temperature may have negative effects on the adsorption. At higher temperatures, the favorable intermolecular forces between adsorbate and adsorbent are much stronger than those between adsorbate and solvent. As a result, the temperature increasing causes the adsorbate to be easier to adsorb. However, our studies indicated no difference in the adsorption properties of the polymer between the temperature range of 36 and 42 °C, indicating no changes in the surface-active sites between that range. Other approaches such as evaluation of binding above and below glass transition temperatures that affect the morphology of amorphous solids[92,93] could provide evidence for or against the specific binding of MIP.

By using ruminal fluid (pH 6.8) as media, a representation of adsorption efficacy of polymers to ETA in complex media was evaluated. Rumen fluid is a complex medium that includes feed residues, microbes, phenolic compounds, organic acids, soluble proteins, peptides, amino acids, etc.[94] The adsorption efficiency of imprinted polymer to its template (ETA) in the presence of compounds that can interact via hydrophobic and π-stacking (phenolic compounds) may indicate its selectivity to the template. Generally, the concentration of ergovaline in naturally contaminated tall fescue seed and forage ranges between 300 and 7000 μg/kg of dry matter.[95] In the present study, the calculated mean ETA concentration in the ruminal

https://doi.org/10.1021/acsomega.1c02158
ACS Omega 2021, 6, 30260−30280

fluid was 3.3 μg/mL, which is one to two orders of magnitude greater than ergovaline concentrations that would be normally expected in the rumen fluid of animals grazing endophyte-infected tall fescue pasture. Since both ergovaline and ETA are ergopeptide alkaloids that have similar ergoline structure and pharmacodynamic properties,[96,97] ETA was used as the reference alkaloid in the present binding studies. The mean adsorption of the NIP was almost 10 percentage points lower than that of MIP, and this phenomenon could be attributed to better specificity along with larger surface area available for adsorption from MIP compared to NIP.

To identify and confirm the nature of the interactions contributing to its adsorption, the Fourier transform infrared spectral information for the [MIP + ETA] complex compared to the MIP polymer was used. The FTIR spectra suggested the presence of additional ring structures in the MIP backbone after the adsorption of ETA. These findings indicate that a significant degree of interaction between the template and the styrene was governed by $\pi-\pi$ stacking. The change in the intensity at 3400 cm^{-1} wavenumbers indicates the involvement of O−H, and/or the N−H stretch in the interaction. In addition, there was a slight change in the intensity for the ester C═O suggesting an inconsequential effect of the ester in template recognition. These experimental data confirmed the identity of the chemical interactions characterized by molecular mechanics and *in silico* docking affinity measurement, further highlighting the importance of $\pi-\pi$ interactions due to the multiplicity of benzene rings on ETA and styrene. Additionally, the changes in the signal intensity of the CH_3 stretching frequency (2955 cm^{-1}) can be explained by a hydrophobic interaction of polymer compounds with neighboring template molecules in the solution. The greater signal due to the presence of water molecules surrounding the CH_3 groups may also indicate the contribution of hydrophobic effects to the adsorption. Similar findings on the influence of water molecules on the hydrophobic effects have been shown and theoretically confirmed.[98,99]

Thus, imprinted polymers have properties conducive to their use as a sorbent in analytical extraction to evaluate the feed or the fate of alkaloids during ruminal digestion that could provide mechanistic clues to the understanding of their toxicokinetic and associated toxicological implications. The compositional characteristics of a MIP could also find use in the production of sensors as described by Bai et al. (2020),[100] which could be utilized to effectively track the alkaloids in the digestive tract. Similarly, Ramakers et al. (2019)[101] developed a laser-grafted molecularly imprinted polymer-based sensor for the detection of histamine to reveal unknown pathological pathways of inflammatory bowel diseases. Such analytical capability could provide aids for the surveillance of the presence of toxins such as alkaloids that could be then further used in precision animal agriculture to develop early stage exposure and diagnose early onset of ergotism. Applications of MIPs to sensor technology have been well utilized in different analytical methods according to the transducers that convert the signals of polymer recognition into physical ones.[102] Additionally, several strategies utilizing molecular imprinting-based solid phase extraction prior to chromatographic analysis for the sample cleanup have been well established.[103] Therefore, a molecularly imprinted polymer, with the optimal binding condition, could represent a useful tool for sample extraction or purification in analytical chromatography and/or as a specific binder to reduce bioavailability in the rumen to mitigate alkaloid toxicity.

CONCLUSIONS

A styrene-based imprinted polymer synthesized with ergotamine as the template was tested for morphological and adsorption properties. MIP had almost twice the external surface area and pore volume compared to NIP, confirmed by the smaller pore size of MIP. The particle size distribution was trimodal with particles of a mean size of 50 μm. Particle morphology determined using SEM and TEM suggested a highly porous nature of MIP. Exposure of polymers to high electron beam (TEM) for 5 min caused the crystallization of polymers. The molecules at the border were under motion, which suggested the presence of amorphous polystyrene chains that may have allowed chain propagation during the polymer synthesis, and these surface molecules crystallized under a high electron beam, indicating the presence of polystyrene chains on the external surface and cross-linkers at the core. This phenomenon would provide more flexibility to the polymers during the adsorption process.

The tetracyclic group of ETA was used as a representative molecule for structural recognition in the polymer. Results suggested that functional groups including indole NH, carbonyl, and hydroxyl groups present on the template molecule can contribute to the physical interaction with the polymers via hydrogen bonding, while the resonance property of styrene ring structures of the polymer and the ring structure in ETA could contribute to π-stacking interactions. Additionally, an alkylphenolic chain in the polymer provided more adsorptive surface area and may be responsible for hydrophobic interactions. Langmuir isotherms indicated that both polymers had favorable adsorption due to similar surface functional groups that are normally present irrespective of imprinting. However, MIP had numerically higher adsorption capacity than NIP, and in addition, MIP exhibited better adsorption efficiency toward ergotamine in rumen fluid compared to NIP, indicating better selectivity of adsorption in a complex *in situ* environment. Additionally, the higher binding efficiency of MIP at low levels of ETA could be due to cavities created during imprinting and greater surface area. Ergopeptides exhibited better adsorption parameters compared to ergoline molecules, indicating the importance of functional groups on the ergoline ring, including a tripeptide moiety. Therefore, this imprinted polymer could be useful for sample purification in affinity chromatography, could be utilized in biosensors for monitoring ergotism in cattle, or could be used in toxicological studies to determine alkaloid pharmacokinetics or -dynamics.

EXPERIMENTAL SECTION

Chemicals. Ethylene glycol dimethacrylate (EGDMA, ≥97%), 2-hydroxyethyl methacrylate (HEMA, >98%), 1,1,3,3-tetramethylguanidine (TMG, >97%), styrene (≥99%), and 2,2-azobisisobutyronitrile (AIBN, ≥98%) were purchased from Fluka (Sigma-Aldrich, Milwaukee, WI, USA). 2-Bromo-α-ergocryptine methanesulfonate (BC), methylergonovine maleate (ME), ergotamine D-tartrate (ETA), and lysergol (LY) were purchased in purified crystalline form (≥97%) from Sigma-Aldrich (St. Louis, MO, USA). Solvents used in polymer synthesis and analytical methods, including methanol (HPLC grade), acetonitrile (optima grade), and acetic and

https://doi.org/10.1021/acsomega.1c02158
ACS Omega 2021, 6, 30260−30280

formic acids (reagent grade), were purchased from Fisher Scientific (Fair Lawn, NJ, USA). The high-purity water used in all experiments was obtained from a Milli-Q Ultra-pure water purification system (Millipore Corporation, Bedford, MA, USA).

The fungal mycotoxin standards—cyclopiazonic acid (CPA), aflatoxin B1 (AFB1), ochratoxin A (OTA), deoxynivalenol (DON), fusaric acid (FA), zearalenone (ZEA), roquefortine C (ROQC), and sterigmatocystin (STG)—were purchased from Sigma-Aldrich (St. Louis, MO, USA). Diacetoxyscirpenol (DAS) was purchased from Biopure (Tulln, Austria). Individual standard stock solutions of mycotoxins (1 mg/mL) were prepared in methanol and stored at −20 °C in the dark until use. Working solutions of studied compounds were prepared from individual stock solutions by dilution with 0.1 M phosphate buffer of pH 6.8. All the experiments were conducted in silanized tubes to reduce the interaction of toxins with glass surface.

Synthesis of Polymers. Imprinted polymers were synthesized by self-assembly bulk polymerization using ETA as the molecular template, styrene and HEMA as functional monomers, EGDMA as the cross-linker, AIBN as the free radical initiator, and toluene as the porogen. Ergotamine tartrate was neutralized by adding 0.6 g of TMG during polymer synthesis to generate the free base form of ETA. Solutions including styrene, HEMA, and EGDMA were distilled under vacuum prior to use to remove inhibitors.

Ergotamine D-tartrate (0.005 mol) was dissolved in 10 mL of methanol containing 0.005 mol of TMG in a 250 mL triple-neck borosilicate round-bottom reactor. Monomers including styrene (0.08 mol) and HEMA (0.04 mol) were added and mixed for 30 min. After mixing, toluene (75 mL) and the cross-linker (EGDMA: 0.1 mol) were added. Nitrogen was purged through the solution throughout the entire procedure. The mixture was heated in an oil bath to 65 °C, and AIBN was added to initiate polymerization and the formation of the MIP. The corresponding NIP was synthesized using the same procedure without the ETA template. The polymerization reaction was stopped after 5 h, and the polymers were subjected to a template washing procedure.

To remove the template, polymer mixtures were filtered through a 0.2 μm filter (Celite 577TM, World Minerals Inc., Santa Barbara, CA, USA) and the filtrate was collected and analyzed for ETA concentration. Template molecules trapped in the polymer matrix were washed successively with the organic solvent (0.2 M HCL in methanol, 100% methanol and 100% acetonitrile) and later stabilized in deionized water. Each template wash procedure was carried out with 100 mL of the solvent with vigorous shaking (15 min) and sonication (15 min) followed by centrifugation (7263*g* for 30 min) and filtration of supernatant. The removal was considered complete when the bleeding of ETA was reduced to nondetectable as confirmed by UPLC−MS/MS analysis of the different consecutive washings. After template removal, the polymers were freeze-dried (<100 mT, −46 °C for 48 h), oven-dried (60 °C overnight), and weighed. The dried polymer was ground to a fine powder using a mortar and pestle and sieved using standard metal sieves (VWR-USA Standard Testing Sieves. IL, USA) to obtain a <250 μm particle size fraction.

Morphological Characterization of Polymers. *Nitrogen Sorption Porosimetry.* Polymers were evaluated for pore size distribution, pore volume, and specific surface area using nitrogen adsorption/desorption isotherms at −196.15 °C according to the Brunauer−Emmett−Teller (BET) procedure.[104] Briefly, a 15.0 mg sample was heat treated (100 °C) for 3 h under inert gas flow to remove atmospheric contaminants. The sample was then cooled, degassed under vacuum (1×10^{-5} Torr), and exposed to increasing nitrogen gas pressures. Nitrogen gas adsorption/desorption was measured under cryogenic conditions using an Autosorb-1C (Quantachrome Instruments, FL, USA) gas sorption analyzer. The BET surface areas were calculated from the adsorption isotherms in the relative pressure range from 0.06 to 0.2 psi. Pore size distribution and total pore volume were determined using the Barrett−Joyner−Halenda method.[105]

Microscopy. A field emission scanning electron microscope (TEM, JEOL 2010F, JEOL, Tokyo, Japan) operating at 200 kV was used to monitor the topography of polymers. As sample preparation procedure, the polymer (5 mg) was suspended in methanol (10 mL), sonicated (35 °C for 10 min), dispersed on a carbon-coated microscopic copper grid (200 μm mesh size), and dried under vacuum at room temperature. Additional morphological characteristics were investigated by scanning electron microscopy (SEM, Hitachi S-4300, Tokyo, Japan). Polymer samples were spread on carbon tape and sputtered with gold (Emscope SC400 Quorum technologies Ltd., East Sussex, UK) before loading onto an aluminum disc. Samples were exposed to 15 keV beam under an aperture width of 2.80 μm with automatic filament saturation.

Dynamic Light Scattering (DLS). For the hydrodynamic diameters of the polymers, samples were suspended in double-distilled water (0.1 mg/mL) or in 5% aqueous methanol and sonicated (1 min, 22 °C). Particle size distribution was measured using continuous wide-angle dynamic light scattering detection (SALD-7101, Nanoparticle size analyzer, Shimadzu Scientific Instruments, Columbia, MD, USA) using a UV laser as the light source (wavelength 375 nm). The instrument was set to make 15 measurements between 0.5 and 300 μm under automatic mode, and diffraction data were obtained as the volume percentage of particle versus the particle size. A reference spectrum of the solvent under similar conditions was used to correct for background noise.

Adsorption Studies. *Isothermal Adsorption.* Isothermal adsorption studies using polymers and the template were conducted in equilibration media consisting of 0.1 M phosphate buffer, pH 6.8. One milligram of the polymer was exposed to increasing concentrations of ETA (Co: 0.00, 0.15, 0.76, 1.52, 7.61, and 15.23 μmol/L) in 10 mL of equilibration media (V). To achieve 1 mg of the polymer in the adsorption media, a 1 L polymer slurry at the rate of 1 mg/mL was made initially and 1 mL aliquot was added to 9 mL of the toxin solution. Samples were incubated (39 °C, 90 min) on a horizontal shaker and then centrifuged (14,500*g*, 10 min) to separate the free ETA from the ETA−polymer complex according to the published protocol.[17] The supernatants were analyzed for ETA (Ce, μmol/L) by high-pressure liquid chromatography equipped with a fluorescence detector (250/420 nm $\lambda_{em}/\lambda_{ex}$, Alliance, Waters Corp., Milford, MA, USA). The amount of ETA adsorbed per unit of polymer was determined by the difference between control and supernatant ETA concentrations as defined in eq 1:

$$q_e = (C_o - C_e)V/W \quad (1)$$

where q_e is the amount adsorbed (μmol/mg); V is the volume (mL); C_o and C_e are initial and equilibrium ETA

https://doi.org/10.1021/acsomega.1c02158
ACS Omega 2021, 6, 30260−30280

concentrations (μmol/L), respectively; and W is the weight of the polymer (mg).

The adsorption properties of the polymers were evaluated by nonlinear regression models including Langmuir and Freundlich (Table 2). Isothermal adsorption parameters from the Langmuir model including adsorption constant (K_L), maximum monolayer adsorption capacity of the adsorbent (Q_o), and adsorption favorability constant (R_L), and Freundlich adsorption parameters including extent of adsorption (K_f) and surface heterogeneity or adsorption intensity (n) were determined (GraphPad Prism Software, version 5.0, USA, or Datafit software, Datafit version 8.1.69, Oakdale Engineering, Oakdale, PA, USA). The best fits were ascertained using correlation coefficients and the lowest residual variance. The model that described the adsorption parameters was selected based on the lowest absolute sum of squares of residuals or the probability of fit for one model versus the other that was determined using the bias-corrected Akaike information criterion (AICc) for the two models (GraphPad Software Inc., La Jolla, CA, USA).

Selectivity. To evaluate the selectivity of MIP for ETA, a study was conducted in 0.01 M ammonium citrate buffer at pH 6.7 containing structurally related alkaloids (Figure 12). A

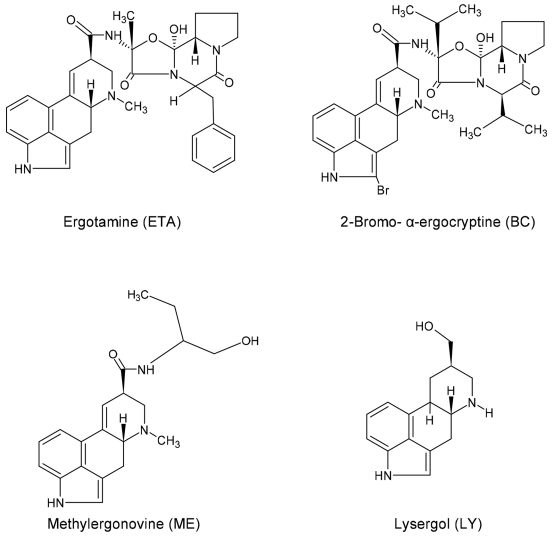

Figure 12. Molecular structures of different ergot alkaloids used in the selectivity experiment.

mixture of four different ergot alkaloids (15 μg/mL) corresponding to different molar concentrations of each toxin (ETA: 11.42, BC: 19.98, ME: 32.93, and LY: 58.97 μmol/L) was prepared in 10 mL buffer and serially diluted (5×) by a factor of 2 to obtain six levels of alkaloid mixture. Also, a control solution was prepared without alkaloids. Polymers (0.1 mg/mL) were added to increasing concentrations of alkaloid mixtures and incubated for 90 min at 39 °C. The samples were centrifuged (14,500g, 10 min), and the supernatant was analyzed for alkaloids using ultra-pressure liquid chromatography coupled to tandem mass spectrometry (UPLC−MS/MS). The selectivity of each alkaloid was evaluated using the adsorption coefficient (k) for each alkaloid calculated using eq 2:

$$k = \frac{[\mathrm{Co} - \mathrm{Ce}]}{M} \times V \tag{2}$$

where C_o and C_e are the initial and final equilibrium concentrations of ergot alkaloids (μmol/L), V is the volume of adsorption medium in liters, and M is the amount of polymer used in the medium in grams. The selectivity for the adsorption of ETA in the presence of other alkaloids was estimated by the selectivity coefficient (k') using eq 3:

$$k' = \frac{k(\mathrm{ETA})}{k(\mathrm{alkaloids})} \tag{3}$$

where alkaloids tested were BC, ME, and LY. The effect of imprinting on selectivity (k'') was determined by the ratio of selectivity coefficients of imprinted to non-imprinted polymer within each alkaloid using eq 4:

$$k'' = \frac{k'\mathrm{imprinted}}{k'\mathrm{non-imprinted}} \tag{4}$$

Cross-Reactivity. The cross-reactivity of the polymers with other structurally diverse contaminants such as mycotoxins was evaluated. A working solution was prepared with increasing concentrations of different selected toxins—CPA, AFB1, OTA, DON, FA, DAS, ZEA, RoqC, and STG—from individual stock solutions (1 g/L in methanol) in 0.01 M ammonium citrate buffer at pH 6.7. A 9 mL working solution for each tested concentration was individually mixed with 1 mL of an adsorbent slurry (1 g/L) in triplicate. The initial mycotoxin range was chosen based on natural levels of contamination[106,107] and matching detectable and quantifiable concentrations assuming 95% adsorption. The tested mycotoxin range included ETA at 0.0625 to 1.5 mg/L; CPA at 12.5 to 300 μg/L; AFB1 and OTA at 7 to 150 μg/L; DON and FA at 42 to 978 μg/L; DAS and ZEA at 14 to 334 μg/L; RoqC at 4 to 100 μg/L; and STG at 11 to 250 μg/L. Along with the samples, three controls were prepared: the buffer solution (blank control) containing no toxin and no adsorbent; a toxin working solution for each tested concentration (toxin control); and a sample containing only the adsorbent in the buffer (sample control). Samples and controls were capped and incubated (39 °C, 90 min) with shaking (150 rpm). After incubation, the samples were centrifuged (14,500g, 10 min) to separate the polymer−toxin complex from the free toxin. The supernatant was analyzed for all toxin concentrations using UPLC−MS/MS. The amount of mycotoxin adsorbed was determined by the difference in concentration between the toxin control and the test sample with the same initial loadings.

Effect of pH and Temperature. To determine the effect of pH, an adsorption study was conducted in 0.1 M potassium phosphate buffer (pH 2, 3, 4, 5, 6, 7, 8, 9, and 10) using a single ETA concentration of 1 mg/L and a polymer concentration of 0.1 mg/mL. The polymer level of 0.1 mg/mL was achieved as described in the isothermal adsorption study. The samples were incubated for 90 min at 39 °C on a horizontal shaker (150 rpm). After the reaction, samples were centrifuged (14,500g, 10 min) to separate the adsorbent−toxin complex from the free toxin. The supernatant was analyzed for free ETA by UPLC−MS/MS, and the adsorption was calculated by taking the difference between the toxin controls and the test samples.

The effect of temperature was determined by adsorption studies performed at 36, 39, and 42 °C. The polymer (0.1 mg/mL prepared as described in the previous paragraph) was exposed to 1 mg/L ETA in 10 mL 0.1 M potassium phosphate buffer (pH 6.8) at each temperature for 90 min on a horizontal

https://doi.org/10.1021/acsomega.1c02158
ACS Omega 2021, 6, 30260−30280

shaker (150 rpm). After the reaction, samples were centrifuged (14,500*g*, 10 min) to separate the adsorbent−toxin complex from the free toxin. The supernatant was analyzed for free ETA by HPLC-FLD, and adsorption was calculated by the difference between toxin controls and tested samples with the measured ETA remaining in the supernatant.

Adsorption in the Rumen Fluid Solution. The adsorption efficiency of different levels of MIP to ETA in comparison to NIP in rumen fluid was determined to evaluate the effect of a complex matrix on adsorption. Ruminal fluid was collected from fistulated steers grazing on endophyte-free fescue pasture. The animals were gathered from the pasture 2 h before collection of rumen fluid. Approximately 1.5 to 2 L of ruminal fluid was collected and filtered through four layers of cheesecloth into a warm (39 °C) 1 L thermos flask. Ruminal fluid was then autoclaved (121 °C, 30 min, 15 psi) and centrifuged (7263*g*, 30 min) to remove the sediments. For the adsorption studies, 500 mL of rumen fluid was diluted with 500 mL of McDougall's buffer.[108]

A known and representative concentration of ETA (3.3 mg/L) was subjected to increasing concentrations of the polymer (0.001, 0.01, 0.1, 1, and 2 mg/mL) in 100 mL of rumen fluid. Increasing concentrations of the polymer in ruminal fluid were prepared using a slurry technique, where a stock solution of the polymer (20 g/L rumen fluid) was prepared and diluted in rumen fluid to the required concentration. The stock slurry solution was continuously agitated while dilutions where prepared to prevent sedimentation. The rumen fluid samples were then spiked with 0.33 μL of the ETA stock solution (1 mg/L) to obtain a final concentration of 3.3 mg/L. The samples were incubated for 90 min under agitation (150 rpm, 39 °C) followed by centrifugation (14,500*g*, 10 min) to recover supernatants that were then analyzed for ETA concentration by HPLC-FLD.

Fourier Transform Infrared Analysis. A Fourier transform infrared spectrometer (FTIR, Spectrum 100, PerkinElmer, Shelton, CT, USA) was used to analyze polymers and polymer−template complexes to determine the functional groups involved in interactions according to procedures described for polymer interactions.[109] The spectrometer was equipped with an overhead ATR diamond crystal that was cleaned with alcohol between measurements. A 10 mg sample was placed on the diamond crystal, and absorbance was recorded in the frequency range of 4000 to 600 cm^{-1} for qualitative examination of the vibrational frequencies of functional groups such as C−C, C−H, C═C, O−H, and N−H. For each freeze-dried sample, 10 scans with resolution of 2 cm^{-1} with automatic baseline correction were performed.

Molecular Mechanics and Dynamics Simulation. Molecular mechanics simulations were carried out to measure and characterize docking and molecular interactions that occur between the functional monomer and ETA. The ETA three-dimensional structure was downloaded from the Chemspider compound repository under the permalink record 7930 (Royal Society of Chemistry, Burlington, VT, USA, CSID: 7930, http://www.chemspider.com/Chemical-Structure.7930.html). Styrene, HEMA, and EGDMA monomers and cross-linker were also assessed from the ChemSpider compound repository under their respective permalink records 7220, 12791, and 7077. A selection of monomer candidates that have generally been used for MIP/NIP production[24] was selected for comparison purposes. Construction of short polymeric chains (10 monomeric units) was also carried out using the CHARMM-GUI effective simulation input generator.[110,111] Construction of a polymer in a toluene solvent cubical box of 100 Å side length was performed using CHARMM-GUI and enabled the generation of several input files for further docking experiments. Pore diameter differences between MIP and NIP from BET measurements were considered for the volumetric proportions of chains present in the box. Molecular docking was performed using AutoDock Vina (v1.5.6, The Scripps Research Institute, La Jolla, CA, USA)[112] between the ligand (ETA) and the receptor (monomer or polymeric material) for the monomers and cross-linkers used in the study herein as well as an array of monomeric materials. With four rotatable bounds, the flexibility of the ETA molecule was preserved during the experiment. A grid box was set up with a 60.0 Å spacing along the *x*, *y*, and z axes, centered on the receptor (monomer) molecule. Mol files were sequentially converted into pdb and pdbqt extension files. The docking experiment was run under C++ generic programming in a Microsoft Windows (10 Pro, 1809, Microsoft Corporation, Redmond, WA, USA) environment and resulted in nine binding modes with a maximum energy range of 3 kcal/mol, producing an affinity measurement (kcal/mol) and distances from the best modes (RMSD).

PyMOL (The PyMOL Molecular Graphics System, v2.2.3 Schrödinger, LLC, New York, NY, USA) was utilized for visualization of the 3D molecular structures for all stages of molecular mechanics simulations and initial tridimensional optimization under the Merck Molecular Force Field (MMFF94). The Chemicalize Chemoinformatic platform was used to evaluate the chemical properties of ETA and tested monomers (ChemAxon, Cambridge, MA, USA, http://www.chemaxon.com).

Analytical Method. Alkaloids and mycotoxins were analyzed using a UPLC−MS/MS system (Acquity Xevo TQD, Waters Corp., Milford, MA, USA) fitted with an electrospray ionization source operated in positive ion mode (ESI+). Analyses were performed by means of a multi-reaction monitoring experiment (MRM) targeting analytes' parent and daughter ions within their specific retention window. Chromatographic separations were performed using 1.7 μm ethylene-bridged C18 hybrid (BEH) particle columns (2.1 × 100 mm, Waters Corp, Milford, MA, USA) maintained at 40 °C. A two-solvent gradient mobile phase composed of water (eluent A) and methanol (eluent B), both acidified with 0.1% formic acid, was used at a flow rate of 0.42 mL/min. A volume of 10 μL of each sample was injected into the system using an autosampler. The elution gradient started at 5% B for the first 2 min followed by a linear increase to 10% B for 2 min and then to 75% B for the next 8 min, then ramped to 99% B in 2 min and brought back to 5% in 2 min, and finally re-equilibrated for 2 min with 5% B. Nitrogen (Nitroflow, Parker-Balston, Haverhill, MA, USA) was used as desolvation and cone gas.[113] Data integration and analysis were performed using MassLynx and QuantLynx data systems (Waters Corp., Milford, MA, USA).

A series 2695 Alliance HPLC separation module (Waters, Milford, MA, USA) equipped with a quaternary pump, an autosampler, and a 474-scanning fluorescence detector (λ_{ex} 250 nm, λ_{em} 420 nm, gain 16, and attenuation 1000) was used to detect ergot alkaloids. Chromatographic data were integrated using the Waters Empower 3 software 7.00.00.99 (Waters, Milford, MA, USA). HPLC separations were performed with a 100 × 4.6 mm i.d., 2.6 μm particle size,

https://doi.org/10.1021/acsomega.1c02158
ACS Omega 2021, 6, 30260−30280

Kinetex C18 column (Phenomenex, Torrance, CA, USA) with a gradient elution consisting of two mobile phases, (A) water and (B) acetonitrile, both spiked with ammonium hydroxide (0.04%). Initial gradient conditions were 100% A held for 1 min, increased linearly to 100% B over 12 min, and held for 3 min. The final step was a linear return to initial conditions over 3 min, which was then held for 2 min for a total run time of 23 min. The sample injection volume was 50 μL. Samples were evaporated to near dryness, and the residue was reconstituted in methanol/water (50/50) and analyzed.[114]

Statistical Analysis. Results of the *in vitro* adsorption studies were analyzed with the GLM procedure (SAS Institute Inc., Cary, NC, USA). Triplicate samples were averaged for statistical analysis. The model included the concentration of analyte, type of analyte, adsorbent concentration, and interaction of analyte concentration × type of analyte. Least square means were calculated for the analyte concentration, type of analyte, and analyte concentration × type of analyte interaction. The adsorption models were compared using the Akaike information criterion (AIC) for the best fit model[115] using GraphPad (GraphPad Prism Software, version 5.0, La Jolla, CA, USA).[83]

AUTHOR INFORMATION

Corresponding Author

Manoj B. Kudupoje − *Chemistry and Toxicology Division, Center for animal Nutrigenomics & Applied Animal Nutrition, Alltech Inc., Nicholasville, Kentucky 40356, United States; Department of Animal and Food Sciences, University of Kentucky, Lexington, Kentucky 40546-0215, United States;* orcid.org/0000-0002-5509-5559; Email: mkudupoje@alltech.com

Authors

Eric S. Vanzant − *Department of Animal and Food Sciences, University of Kentucky, Lexington, Kentucky 40546-0215, United States*

Kyle R. McLeod − *Department of Animal and Food Sciences, University of Kentucky, Lexington, Kentucky 40546-0215, United States*

Alexandros Yiannikouris − *Chemistry and Toxicology Division, Center for animal Nutrigenomics & Applied Animal Nutrition, Alltech Inc., Nicholasville, Kentucky 40356, United States*

Complete contact information is available at: https://pubs.acs.org/10.1021/acsomega.1c02158

Author Contributions

Eric S. Vanzant, Alexandros Yiannikouris, and Kyle R. McLeod oversaw experiments. Eric S. Vanzant and Manoj B. Kudupoje analyzed the data and wrote the paper. Alexandros Yiannikouris provided material support, performed experiments, and contributed to manuscript revisions.

Funding

This work was funded and co-supported by Alltech Inc. and the University of Kentucky through the Alltech-UKY Research Alliance Programs.

Notes

The authors declare no competing financial interest.

REFERENCES

(1) Hoveland, C. S. Importance and economic significance of the Acremonium endophytes to performance of animals and grass plant. *Agric., Ecosyst. Environ.* **1993**, *44*, 3−12.

(2) Rodriguez, R. J.; White, J. F., Jr.; Arnold, A. E.; Redman, R. S. Fungal endophytes: diversity and functional roles. *New Phytol.* **2009**, *182*, 314−330.

(3) Strickland, J. R.; Oliver, J. W.; Cross, D. L. Fescue toxicosis and its impact on animal agriculture. *Vet. Hum. Toxicol.* **1993**, *35*, 454−464.

(4) Schmidt, S. P.; Hoveland, C. S.; Clark, E. M.; Davis, N. D.; Smith, L. A.; Grimes, H. W.; Holliman, J. L. Association of an endophytic fungus with fescue toxicity in steers fed Kentucky 31 tall fescue seed or hay. *J. Anim. Sci.* **1982**, *55*, 1259−1263.

(5) Mantegani, S.; Brambilla, E.; Varasi, M. Ergoline derivatives: receptor affinity and selectivity. *Farmaco* **1999**, *54*, 288−296.

(6) Gornemann, T.; Jähnichen, S.; Schurad, B.; Latté, K. P.; Horowski, R.; Tack, J.; Flieger, M.; Pertz, H. H. Pharmacological properties of a wide array of ergolines at functional alpha(1)-adrenoceptor subtypes. *Naunyn-Schmiedeberg's Arch. Pharmacol.* **2008**, *376*, 321−330.

(7) Rowell, P. P.; Larson, B. T. Ergocryptine and other ergot alkaloids stimulate the release of [3H]dopamine from rat striatal synaptosomes. *J. Anim. Sci.* **1999**, *77*, 1800−1806.

(8) Strickland, J. R.; Looper, M. L.; Matthews, J. C.; Rosenkrans, C. F., Jr.; Flythe, M. D.; Brown, K. R. Board-invited review: St. Anthony's Fire in livestock: causes, mechanisms, and potential solutions. *J. Anim. Sci.* **2011**, *89*, 1603−1626.

(9) Foote, A. P.; Harmon, D. L.; Strickland, J. R.; Bush, L. P.; Klotz, J. L. Effect of ergot alkaloids on contractility of bovine right ruminal artery and vein. *J. Anim. Sci.* **2011**, *89*, 2944−2949.

(10) Mulac, D.; Humpf, H. U. Cytotoxicity and accumulation of ergot alkaloids in human primary cells. *Toxicology* **2011**, *282*, 112−121.

(11) Repussard, C.; Zbib, N.; Tardieu, D.; Guerre, P. Endophyte infection of tall fescue and the impact of climatic factors on ergovaline concentrations in field crops cultivated in southern France. *J. Agric. Food Chem.* **2014**, *62*, 9609−9614.

(12) Di Mavungu, J. D.; Malysheva, S. V.; Sanders, M.; Larionova, D.; Robbens, J.; Dubruel, P.; Van Peteghem, C.; De Saeger, S. Development and validation of a new LC−MS/MS method for the simultaneous determination of six major ergot alkaloids and their corresponding epimers. Application to some food and feed commodities. *Food Chem.* **2012**, *135*, 292−303.

(13) Furey, A.; Moriarty, M.; Bane, V.; Kinsella, B.; Lehane, M. Ion suppression; a critical review on causes, evaluation, prevention and applications. *Talanta* **2013**, *115*, 104−122.

(14) Matuszewski, B. K.; Constanzer, M. L.; Chavez-Eng, C. M. Strategies for the assessment of matrix effect in quantitative bioanalytical methods based on HPLC-MS/MS. *Anal. Chem.* **2003**, *75*, 3019−3030.

(15) Billups, J.; Jones, C.; Jackson, T. L.; Ablordeppey, S. Y.; Spencer, S. D. Simultaneous RP-HPLC-DAD quantification of bromocriptine, haloperidol and its diazepane structural analog in rat plasma with droperidol as internal standard for application to drug-interaction pharmacokinetics. *Biomed. Chromatogr.* **2010**, *24*, 699−705.

(16) Webb, K. S.; Baker, P. B.; Cassells, N. P.; Francis, J. M.; Johnston, D.; Lancaster, S.; Minty, P.; Reed, G.; White, S. The analysis of lysergide (LSD): The development of novel enzyme immunoassay and immunoaffinity extraction procedures together with an HPLC-MS confirmation procedure. *J. Forensic Sci.* **1996**, *41*, 938−946.

(17) Lenain, P.; Diana Di Mavungu, J.; Dubruel, P.; Robbens, J.; De Saeger, S. Development of suspension polymerized molecularly imprinted beads with metergoline as template and application in a solid-phase extraction procedure toward ergot alkaloids. *Anal. Chem.* **2012**, *84*, 10411−10418.

(18) Sellergren, B.; Andersson, L. I. Application of imprinted synthetic polymers in binding assay development. *Methods* **2000**, *22*, 92−106.
(19) Lian, Z.; Liang, Z.; Wang, J. Selective extraction and concentration of mebendazole in seawater samples using molecularly imprinted polymer as sorbent. *Mar. Pollut. Bull.* **2015**, *91*, 96−101.
(20) Rampey, A. M.; Umpleby, R. J.; Rushton, G. T.; Iseman, J. C.; Shah, R. N.; Shimizu, K. D. Characterization of the imprint effect and the influence of imprinting conditions on affinity, capacity, and heterogeneity in molecularly imprinted polymers using the Freundlich isotherm-affinity distribution analysis. *Anal. Chem.* **2004**, *76*, 1123−1133.
(21) Sun, Z.; Schüssler, W.; Sengl, M.; Niessner, R.; Knopp, D. Selective trace analysis of diclofenac in surface and wastewater samples using solid-phase extraction with a new molecularly imprinted polymer. *Anal. Chim. Acta* **2008**, *620*, 73−81.
(22) Barde, L. N.; Ghule, M. M.; Roy, A. A.; Mathur, V. B.; Shivhare, U. D. Development of molecularly imprinted polymer as sustain release drug carrier for propranolol HCL. *Drug Dev. Ind. Pharm.* **2013**, *39*, 1247−1253.
(23) Chapuis-Hugon, F.; Cruz-Vera, M.; Savane, R.; Ali, W. H.; Valcarcel, M.; Deveaux, M.; Pichon, V. Selective sample pretreatment by molecularly imprinted polymer for the determination of LSD in biological fluids. *J. Sep. Sci.* **2009**, *32*, 3301−3309.
(24) Vasapollo, G.; Del Sole, R.; Mergola, L.; Lazzoi, M. R.; Scardino, A.; Scorrano, S.; Mele, G. Review: Molecularly Imprinted Polymers: Present and Future Prospective. *Int. J. Mol. Sci.* **2011**, *12*, 5908−5945.
(25) Klotz, J. L. Activities and effects of ergot alkaloids on livestock physiology and production. *Toxins* **2015 Aug**, *7*, 2801−2821.
(26) Ayers, A. W.; Hill, N. S.; Rottinghaus, G. E.; Stuedemann, J. A.; Thompson, F. N.; Purinton, P. T.; Seman, D. H.; Dawe, D. L.; Parks, A. H.; Ensley, D. Ruminal metabolism and transport of tall fescue ergot alkaloids. *Crop Sci.* **2009 Nov**, *49*, 2309−2316.
(27) Hill, N. S.; Thompson, F. N.; Stuedemann, J. A.; Rottinghaus, G. W.; Ju, H. J.; Dawe, D. L.; Hiatt, E. E. Ergot alkaloids transport across ruminant gastric tissues. *J. Anim. Sci.* **2001**, *79*, 542−549.
(28) Karim, K.; Breton, F.; Rouillon, R.; Piletska, E. V.; Guerreiro, A.; Chianella, I.; Piletsky, S. A. How to find effective functional monomers for effective molecularly imprinted polymers? *Adv. Drug Delivery Rev.* **2005**, *57*, 1795−1808.
(29) O'Mahony, J.; Molinelli, A.; Nolan, K.; Smyth, M. R.; Mizaikoff, B. Anatomy of a successful imprint: Analysing the recognition mechanisms of a molecularly imprinted polymer for quercetin. *Biosens. Bioelectron.* **2006**, *21*, 1383−1392.
(30) O'Mahony, J.; Molinelli, A.; Nolan, K.; Smyth, M. R.; Mizaikoff, B. Towards the rational development of molecularly imprinted polymers: 1H NMR studies on hydrophobicity and ion-pair interactions as driving forces for selectivity. *Biosens. Bioelectron.* **2005**, *20*, 1884−1893.
(31) Svenson, J.; Karlsson, J. G.; Nicholls, I. A. 1H nuclear magnetic resonance study of the molecular imprinting of (−)-nicotine: template self-association, a molecular basis for cooperative ligand binding. *J. Chromatogr. A.* **2004**, *1024*, 39−44.
(32) Ekberg, B.; Mosbach, K. Molecular imprinting: A technique for producing specific separation materials. *Trends Biotechnol.* **1989**, *7*, 92−96.
(33) Yu, C.; Mosbach, K. Insights into the origins of binding and the recognition properties of molecularly imprinted polymers prepared using an amide as the hydrogen-bonding functional group. *J. Mol. Recognit.* **1998**, *11*, 69−74.
(34) Yu, C.; Mosbach, K. Influence of mobile phase composition and cross-linking density on the enantiomeric recognition properties of molecularly imprinted polymers. *J. Chromatogr. A.* **2000**, *888*, 63−72.
(35) Moring, S. E.; Wong, O. S.; Stobaugh, J. F. Target specific sample preparation from aqueous extracts with molecular imprinted polymers. *J. Pharm. Biomed. Anal.* **2002**, *27*, 719−728.
(36) Hwang, C. C.; Lee, W. C. Chromatographic characteristics of cholesterol-imprinted polymers prepared by covalent and non-covalent imprinting methods. *J. Chromatogr. A.* **2002**, *962*, 69−78.
(37) Spivak, D. A. Optimization, evaluation, and characterization of molecularly imprinted polymers. *Adv. Drug Delivery Rev.* **2005**, *57*, 1779−1794.
(38) Amin, M.; Sepp, W. Quantitative thin-layer chromatographic analysis of ergotamine tartrate and caffeine in the nanogram range. *J. Chromatogr.* **1976**, *118*, 225−232.
(39) Smith, D.; Smith, L.; Shafer, W.; Klotz, J.; Strickland, J. Development and validation of an LC-MS method for quantitation of ergot alkaloids in lateral saphenous vein tissue. *J. Agric. Food Chem.* **2009**, *57*, 7213−7220.
(40) Krska, R.; Stubbings, G.; Macarthur, R.; Crews, C. Simultaneous determination of six major ergot alkaloids and their epimers in cereals and foodstuffs by LC-MS-MS. *Anal. Bioanal. Chem.* **2008**, *391*, 563−576.
(41) Vojta, D.; Vazdar, M. The study of hydrogen bonding and $\pi\cdots\pi$ interactions in phenol··· ethynylbenzene complex by IR spectroscopy. *Spectrochim. Acta, Part A* **2014**, *132*, 6−14.
(42) Waters, M. L. Aromatic interactions in model systems. *Curr. Opin. Chem. Biol.* **2002**, *6*, 736−741.
(43) Ellwanger, A.; Berggren, C.; Bayoudh, S.; Crecenzi, C.; Karlsson, L.; Owens, P. K.; Ensing, K.; Cormack, P.; Sherrington, D.; Sellergren, B. Evaluation of methods aimed at complete removal of template from molecularly imprinted polymers. *Analyst* **2001**, *126*, 784−792.
(44) Kulikova, G. A.; Ryabinina, I. V.; Guseynov, S. S.; Parfenyuk, E. V. Calorimetric study of adsorption of human serum albumin onto silica powders. *Thermochim. Acta* **2010**, *503*, 65−69.
(45) Li, S.; Cao, S.; Whitcombe, M. J.; Piletsky, S. A. Size matters: challenges in imprinting macromolecules. *Prog. Polym. Sci.* **2014**, *39*, 145−163.
(46) Valdebenito, A.; Espinoza, P.; Lissi, E. A.; Encinas, M. V. Bovine serum albumin as chain transfer agent in the acrylamide polymerization. Protein-polymer conjugates. *Polymer* **2010**, *51*, 2503−2507.
(47) Peng-Ju, W.; Jun, Y.; Qing-De, S.; Yun, G.; Xiao-Lan, Z.; Ji-Bao, C. Rapid removal of template from molecularly imprinted polymers by accelerated solvent extraction. *Chin. J. Anal. Chem.* **2007**, *35*, 484−488.
(48) Lorenzo, R.; Carro, A.; Alvarez-Lorenzo, C.; Concheiro, A. To remove or not to remove? The challenge of extracting the template to make the cavities available in molecularly imprinted polymers (MIPs). *Int. J. Mol. Sci.* **2011**, *12*, 4327−4347.
(49) Hjerten, S.; Liao, J. L.; Nakazato, K.; Wang, Y.; Zamaratskaia, G.; Zhang, H. X. Gels mimicking antibodies in their selective recognition of proteins. *Chromatographia* **1997**, *44*, 227−234.
(50) Flavin, K.; Resmini, M. Imprinted nanomaterials: a new class of synthetic receptors. *Anal.Bioanal. Chem.* **2009**, *393*, 437−444.
(51) Huang, Y. P.; Liu, Z. S.; Zheng, C.; Gao, R. Y. Recent developments of molecularly imprinted polymer in CEC. *Electrophoresis* **2009**, *30*, 155−162.
(52) Verheyen, E.; Schillemans, J. P.; van Wijk, M.; Demeniex, M.-A.; Hennink, W. E.; van Nostrum, C. F. Challenges for the effective molecular imprinting of proteins. *Biomaterials* **2011**, *32*, 3008−3020.
(53) Hawkins, D. M.; Stevenson, D.; Reddy, S. M. Investigation of protein imprinting in hydrogel-based molecularly imprinted polymers (HydroMIPs). *Anal. Chim. Acta.* **2005**, *542*, 61−65.
(54) Bonini, F.; Piletsky, S.; Turner, A. P. F.; Speghini, A.; Bossi, A. Surface imprinted beads for the recognition of human serum albumin. *Biosens. Bioelectron.* **2007**, *22*, 2322−2328.
(55) Tunc, Y.; Hasirci, N.; Yesilada, A.; Ulubayram, K. Comonomer effects on binding performances and morphology of acrylate-based imprinted polymers. *Polymer* **2006**, *47*, 6931−6940.
(56) Sellergren, B. Polymer-and template-related factors influencing the efficiency in molecularly imprinted solid-phase extractions. *TrAC, Trends Anal. Chem.* **1999**, *18*, 164−174.

https://doi.org/10.1021/acsomega.1c02158
ACS Omega 2021, 6, 30260−30280

(57) Nantasenamat, C.; Isarankura-Na-Ayudhya, C.; Bülow, L.; Ye, L.; Prachayasittikul, V. In silico design for synthesis of molecularly imprinted microspheres specific towards bisphenol A by precipitation polymerization. *EXCLI J.* **2006**, *5*, 103−117.
(58) Matyjaszewski, K.; Davis, T. P.: *Handbook of radical polymerization; ISBN: 978−0−471-39274-3*; John Wiley & Sons, Inc., 2002. 845−893
(59) Lanza, F.; Rüther, M.; Hall, A. J.; Dauwe, C.; Sellergren, B. Studies on the process of formation, nature and stability of binding sites in molecularly imprinted polymers. *MRS Online Proc. Libr.* **2002**, *723*, 561−5611.
(60) Turner, N. W.; Holdsworth, C. I.; Donne, S. W.; McCluskey, A.; Bowyer, M. C. Microwave induced MIP synthesis: comparative analysis of thermal and microwave induced polymerisation of caffeine imprinted polymers. *New J.Chem.* **2010**, *34*, 686−692.
(61) Sellergren, B.; Shea, K. J. Influence of polymer morphology on the ability of imprinted network polymers to resolve enantiomers. *J. Chromatogr. A* **1993**, *635*, 31−49.
(62) Umpleby, R. J.; Baxter, S. C.; Chen, Y.; Shah, R. N.; Shimizu, K. D. Characterization of molecularly imprinted polymers with the Langmuir-Freundlich isotherm. *Anal. Chem.* **2001**, *73*, 4584−4591.
(63) Belton, G. Langmuir adsorption, the Gibbs adsorption isotherm, and interracial kinetics in liquid metal systems. *Metall. Trans. B* **1976**, *7*, 35−42.
(64) Hall, K. R.; Eagleton, L. C.; Acrivos, A.; Vermeulen, T. Pore- and solid-diffusion kinetics in fixed-bed adsorption under constant-pattern conditions. *Ind. Eng. Chem. Fundam.* **1966**, *5*, 212−223.
(65) Langmuir, I. The adsorption of gases on plane surfaces of glass, mica and platinum. *J. Am. Chem. Soc.* **1918**, *40*, 1362−1403.
(66) Hutson, N. D.; Yang, R. T. Theoretical basis for the Dubinin-Radushkevitch (D-R) adsorption isotherm equation. *Adsorption* **1997**, *3*, 189−195.
(67) Fo, O.; Odebunmi, E. Freundlich and Langmuir isotherms parameters for adsorption of methylene blue by activated carbon derived from agrowastes. *Adv. Nat. Appl. Sci.* **2010**, *4*, 281−288.
(68) Burnham, K. P.; Anderson, D. R. *Statistical theory and numerical results. Model selection and multimodel inference: a practical information-theoretic approach*; 2nd Edition, Springer Science & Business Media, 2003. 421−424
(69) Weber, T. W.; Chakravorti, R. K. Pore and solid diffusion models for fixed-bed adsorbers. *AIChE J.* **1974**, *20*, 228−238.
(70) Graham, D. The characterization of physical adsorption systems I. The equilibrium function and standard free energy of adsorption. *J. Phys. Chem.* **1953**, *57*, 665−669.
(71) Sun, C.-J.; Sun, L.-Z.; Sun, X.-X. Graphical evaluation of the favorability of adsorption processes by using conditional langmuir constant. *Ind. Eng. Chem. Res.* **2013**, *52*, 14251−14260.
(72) Liechty, W. B.; Kryscio, D. R.; Slaughter, B. V.; Peppas, N. A. Polymers for drug delivery systems. *Annu. Rev. Chem. Biomol. Eng.* **2010**, *1*, 149−173.
(73) Clapper, J. D.; Guymon, C. A. Physical behavior of cross-linked PEG hydrogels photopolymerized within nanostructured lyotropic liquid crystalline templates. *Macromolecules* **2007**, *40*, 1101−1107.
(74) Kimhi, O.; Bianco-Peled, H. Microcalorimetry study of the interactions between poly (N-isopropylacrylamide) microgels and amino acids. *Langmuir* **2002**, *18*, 8587−8592.
(75) Kimhi, O.; Bianco-Peled, H. Study of the interactions between protein-imprinted hydrogels and their templates. *Langmuir* **2007**, *23*, 6329−6335.
(76) Janiak, D. S.; Ayyub, O. B.; Kofinas, P. Effects of charge density on the recognition properties of molecularly imprinted polymeric hydrogels. *Macromolecules* **2009**, *42*, 1703−1709.
(77) Oxelbark, J.; Legido-Quigley, C.; Aureliano, C. S.; Titirici, M.-M.; Schillinger, E.; Sellergren, B.; Courtois, J.; Irgum, K.; Dambies, L.; Cormack, P. A.; Sherrington, D. C.; de Lorenzi, E. Chromatographic comparison of bupivacaine imprinted polymers prepared in crushed monolith, microsphere, silica-based composite and capillary monolith formats. *J. Chromatogr. A.* **2007**, *1160*, 215−226.
(78) Schirmer, C.; Meisel, H. Synthesis of a molecularly imprinted polymer for the selective solid-phase extraction of chloramphenicol from honey. *J. Chromatogr. A.* **2006**, *1132*, 325−328.
(79) Pichon, V.; Chapuis-Hugon, F. Role of molecularly imprinted polymers for selective determination of environmental pollutants—a review. *Anal. Chimica Acta.* **2008**, *622*, 48−61.
(80) Zhang, Y.; Qu, X.; Wang, F.; Wu, G.; Li, J.; Hong, H.; Liu, C. Effect of the solvent on improving the recognition properties of surface molecularly imprinted polymers for precise separation of erythromycin. *RSC Adv.* **2015**, *5*, 83619−83627.
(81) Sellergren, B. *The Non-Covalent Approach to Molecular Imprinting. Molecularly imprinted polymers: Man-made mimics of antibodies and their application in analytical chemistry*. ISBN: 9780444828378. 1st Edition. Elsevier Science, 2000; *23*. 101−138
(82) Chen, L.; Xu, S.; Li, J. Recent advances in molecular imprinting technology: current status, challenges and highlighted applications. *Chem. Soc. Rev.* **2011**, *40*, 2922−2942.
(83) Sun, C.-J.; Sun, L.-Z.; Sun, X.-X. Graphical evaluation of the favorability of adsorption processes by using conditional Langmuir constant. *Ind. Eng. Chem. Res.* **2013**, *52* (39), 14251−14260.
(84) Foo, K. Y.; Hameed, B. H. Insights into the modeling of adsorption isotherm systems. *Chem. Eng. J.* **2010**, *156*, 2−10.
(85) Dunicz, B. L. Surface area of activated charcoal by Langmuir adsorption isotherm. *J. Chem. Educ.* **1961**, *38*, 357.
(86) Gryshchenko, A. O.; Bottaro, C. Development of molecularly imprinted polymer in porous film format for binding of phenol and alkylphenols from water. *Int. J. Mol. Sci.* **2014**, *15*, 1338−1357.
(87) Carrott, P. J. M.; Carrott, M. R.; Vale, T. S. C.; Marques, L.; Nabais, J. V.; Mourao, P. A. M.; Suhas, P. A. M. Characterisation of surface ionisation and adsorption of phenol and 4-nitrophenol on non-porous carbon blacks. *Adsorpt. Sci. Technol.* **2008**, *26*, 827−841.
(88) Kim, B.; Peppas, N. A. Synthesis and characterization of pH-sensitive glycopolymers for oral drug delivery systems. *J. Biomater. Sci., Polym. Ed.* **2002**, *13*, 1271−1281.
(89) Yang, S.; Park, K.; Rocca, J. G. Semi-interpenetrating polymer network superporous hydrogels based on poly (3-sulfopropyl acrylate, potassium salt) and poly (vinyl alcohol): synthesis and characterization. *J. Bioact. Compat. Polym.* **2004**, *19*, 81−100.
(90) Schmaljohann, D. Thermo-and pH-responsive polymers in drug delivery. *Adv. Drug Delivery Rev.* **2006**, *58*, 1655−1670.
(91) Reinhardt, M.; Dzubiella, J.; Trapp, M.; Gutfreund, P.; Kreuzer, M.; Gröschel, A. H.; Müller, A. H. E.; Ballauff, M.; Steitz, R. Fine-tuning the structure of stimuli-responsive polymer films by hydrostatic pressure and temperature. *Macromolecules* **2013**, *46*, 6541−6547.
(92) Roos, Y.; Karel, M. Differential scanning calorimetry study of phase transitions affecting the quality of dehydrated materials. *Biotechnol. Prog.* **1990**, *6*, 159−163.
(93) Sablani, S. S.; Kasapis, S.; Rahman, M. S. Evaluating water activity and glass transition concepts for food stability. *J. Food Eng.* **2007**, *78*, 266−271.
(94) Wang, Y.; McAllister, T. A. Rumen microbes, enzymes and feed digestion-A review. *Asian-Australas. J. Anim. Sci.* **2002**, *15*, 1659−1676.
(95) Krska, R.; Crews, C. Significance, chemistry and determination of ergot alkaloids: a review. *Food Addit. Contam.* **2008**, *25*, 722−731.
(96) Porter, J. Analysis of endophyte toxins: fescue and other grasses toxic to livestock. *J. Anim. Sci.* **1995**, *73*, 871−880.
(97) Larson, B. T.; Harmon, D. L.; Piper, E. L.; Griffis, L. M.; Bush, L. P. Alkaloid binding and activation of D2 dopamine receptors in cell culture. *J. Anim. Sci.* **1999**, *77*, 942−947.
(98) Schmidt, P.; Dybal, J.; Trchová, M. Investigations of the hydrophobic and hydrophilic interactions in polymer−water systems by ATR FTIR and Raman spectroscopy. *Vib. Spectrosc.* **2006**, *42*, 278−283.
(99) Schmidt, P.; Dybal, J.; Rodriguez-Cabello, J. C.; Reboto, V. Role of water in structural changes of poly (AVGVP) and poly (GVGVP) studied by FTIR and Raman spectroscopy and ab initio calculations. *Biomacromolecules* **2005**, *6*, 697−706.

https://doi.org/10.1021/acsomega.1c02158
ACS Omega 2021, 6, 30260−30280

(100) Bai, H.; Vyshniakova, K.; Pavlica, E.; Malacco, V. M. R.; Yiannikouris, A.; Yerramreddy, T. R.; Donkin, S. S.; Nawrocki, R. A. Impedimetric, PEDOT: PSS-Based Organic Electrochemical Sensor for Detection of Histamine for Precision Animal Agriculture. *IEEE Sens. J.* **2020**, *4*, 1−4.
(101) Ramakers, G.; Wackers, G.; Trouillet, V.; Welle, A.; Wagner, P.; Junkers, T. Laser-Grafted Molecularly Imprinted Polymers for the Detection of Histamine from Organocatalyzed Atom Transfer Radical Polymerization. *Macromolecules* **2019**, *52*, 2304−2313.
(102) Yano, K.; Karube, I. Molecularly imprinted polymers for biosensor applications. *TrAC, Trends Anal. Chem.* **1999**, *18*, 199−204.
(103) Arabi, M.; Ostovan, A.; Bagheri, A. R.; Guo, X.; Wang, L.; Li, J.; Wang, X.; Li, B.; Chen, L. Strategies of molecular imprinting-based solid-phase extraction prior to chromatographic analysis. *TrAC, Trends Anal. Chem.* **2020**, *128*, 115923.
(104) Brunauer, S.; Emmett, P. H.; Teller, E. Adsorption of gases in multimolecular layers. *J. Am. Chem. Soc.* **1938**, *60*, 309−319.
(105) Barrett, E. P.; Joyner, L. G.; Halenda, P. P. The determination of pore volume and area distributions in porous substances. I. Computations from nitrogen isotherms. *J. Am. Chem. Soc.* **1951**, *73*, 373−380.
(106) Placinta, C. M.; D'mello, J. F.; Macdonald, A. M. C. A review of worldwide contamination of cereal grains and animal feed with Fusarium mycotoxins. *Anim. Feed Sci. Technol.* **1999**, *78*, 21−37.
(107) Binder, E. M.; Tan, L. M.; Chin, L. J.; Handl, J.; Richard, J. Worldwide occurrence of mycotoxins in commodities, feeds and feed ingredients. *Anim. Feed Sci. Technol.* **2007**, *137*, 265−282.
(108) McDougall, E. I. Studies on ruminant saliva. 1. The composition and output of sheep's saliva. *Biochem. J.* **1948**, *43*, 99−109.
(109) Molinelli, A.; O'Mahony, J.; Nolan, K.; Smyth, M. R.; Jakusch, M.; Mizaikoff, B. Analyzing the mechanisms of selectivity in biomimetic self-assemblies via IR and NMR spectroscopy of prepolymerization solutions and molecular dynamics simulations. *Anal. Chem.* **2005**, *77*, 5196−5204.
(110) Jo, S.; Kim, T.; Iyer, V. G.; Im, W. CHARMM-GUI: A Web-based Graphical User Interface for CHARMM. *J. Comput. Chem.* **2008**, *29*, 1859−1865.
(111) Choi, Y. K.; Park, S. J.; Park, S.; Kim, N. R.; Kern, J. L.; Lee, J.; Im, W. CHARMM-GUI Polymer Builder for Modeling and Simulation of Synthetic Polymers. *J. Chem. Theory Comput.* **2021**, *17*, 2431−2443.
(112) Trott, O.; Olson, A. J. AutoDock Vina: improving the speed and accuracy of docking with a new scoring function, efficient optimization and multithreading. *J. Comput. Chem.* **2009**, *31*, 455−461.
(113) Jackson, L. C.; Kudupoje, M. B.; Yiannikouris, A. Simultaneous multiple mycotoxin quantification in feed samples using three isotopically labeled internal standards applied for isotopic dilution and data normalization through ultra-performance liquid chromatography/electrospray ionization tandem mass spectrometry. *Rapid Commun. Mass Spectrom.* **2012**, *26*, 2697−2713.
(114) Rottinghaus, G. E.; Garner, G. B.; Cornell, C. N.; Ellis, J. L. HPLC method for quantitating ergovaline in endophyte-infested tall fescue: seasonal variations of ergovaline levels in stems with leaf sheaths, leaf blades, and seed heads. *J. Agric. Food Chem.* **1991**, *39*, 112−115.
(115) Spiess, A.-N.; Neumeyer, N. An evaluation of R2 as an inadequate measure for nonlinear models in pharmacological and biochemical research: a Monte Carlo approach. *BMC pharmacol.* **2010**, *10*, 6.

https://doi.org/10.1021/acsomega.1c02158
ACS Omega 2021, 6, 30260−30280